Group 3 innate lymphoid cells mediate early protective immunity against *Mycobacterium tuberculosis*

Amanda Ardain[1,2*], Racquel Domingo-Gonzalez[3*], Shibali Das[3*], Samuel W. Kazer[4] , Nicole C. Howard[3], Alveera Singh[1,2], Mushtaq Ahmed[3], Shepherd Nhamoyebonde[1,2], Javier Rangel-Moreno[5], Paul Ogongo[1,2,6], Lan Lu[3], Duran Ramsuran[2], Maria de la Luz Garcia-Hernandez[5], Tyler Ulland[7], Matthew Darby[8], Eugene Park[7,9,], Farina Karim[1], Laura Melocchi[7], Rajhmun Madansein[10], Kaylesh Jay Dullabh[10], Micah Dunlap[3], Nancy Marin-Agudelo[3], Takashi Ebihara[7,9], Thumbi Ndung'u[2], Deepak Kaushal[11], Alexander S. Pym[1,2], Jay K. Kolls[12], Adrie Steyn[1,2], Joaquín Zúñiga[13], William Horsnell[8], Wayne Yokoyama[7,9,14], Alex K. Shalek[4], Henrik N. Kløverpris[1,2,15,16], Marco Colonna[5], Alasdair Leslie[1,2,16*] and Shabaana A. Khader[3*]

[1]Africa Health Research Institute, KwaZulu-Natal, South Africa; [2]School of Laboratory Medicine and Medical Sciences, University of KwaZulu-Natal, South Africa; [3]Department of Molecular Microbiology, Washington University School of Medicine, St. Louis, Missouri, USA; [4]Institute for Medical Engineering and Science and Department of Chemistry, Massachusetts Institute of Technology, Cambridge, Massachusetts, USA; Ragon Institute of MGH, MIT and Harvard, Cambridge, Massachusetts, USA; Broad Institute of MIT and Harvard, Cambridge, Massachusetts, USA. [5]Division of Allergy, Immmunology and Rheumatology, Department of Medicine, Universtiy of Rochester Medical Center, Rochester, New York, USA, [6]Department of Tropical and Infectious Diseases, Institute of Primate Research, Nairobi, Kenya [7]Division of Immunobiology, Department of Pathology and Immunology, Washington University School of Medicine, St. Louis, Missouri, USA; [8]IDM, University of Cape Town, South Africa; [9]Howard Hughes Medical Institute, Washington University School of Medicine, St Louis, Missouri, USA; [10]Department of Cardiothoracic Surgery, Nelson Mandela School of Medicine, University of KwaZulu-Natal, Durban, South Africa; [11]Tulane National Primate Research Center,

Covington, Louisiana, [12]Tulane University Health Sciences, New Orleans, Louisiana, [13]Instituto Nacional de Enfermedades Respiratorias Ismael Cosio Villegas, Mexico City, MX, [14]Division of Rheumatology, Department of Medicine, Washington University School of Medicine, St. Louis, Missouri, USA; [15]Department of Immunology and Microbiology, University of Copenhagen, Denmark; [16]Department of infection and immunity, University College London, UK;

* Contributed equally

For Correspondence:

Shabaana A. Khader

Department of Molecular Microbiology,

Washington University School of Medicine,

St. Louis, Missouri, USA

Email:sakhader@wustl.edu

Alasdair Leslie

Africa Health Research Institute,

KwaZulu-Natal, South Africa

Email: al.leslie@ahri.org

Tuberculosis (TB) is the leading worldwide cause of death by an infectious disease[1]. The involvement of innate lymphoid cells (ILC) in immune responses to *Mycobacterium tuberculosis* (*Mtb*) infection is unknown. We show that circulating ILC subsets are severely depleted from the blood of pulmonary TB (PTB) participants and largely restored upon treatment. PTB infection increased accumulation of all ILC subsets in the human lung, coinciding with a robust transcriptional response to infection, including a role in orchestrating the recruitment of other immune subsets. Using mouse models, we show that Group 3 ILCs (ILC3) accumulated rapidly in the lungs of *Mtb*-infected mice and preceded the accumulation of alevolar macrophages in the lung. Importantly, mice lacking ILC3s exhibit reduced early accumulation of alveolar macrophages and decreased *Mtb* control. The C-X-C Motif Chemokine Receptor 5 (CXCR5)/ C-X-C Motif Chemokine Ligand 13 (CXCL13) axis is implicated in *Mtb* control, as infection upregulated CXCR5 on circulating ILC3s and increased plasma levels of its ligand CXCL13 in humans. Moreover, Interleukin (IL)-23-dependent ILC3 expansion in mice and production of IL-17 and IL-22 were found to be critical inducers of CXCL13 in the lung, early innate immunity, and formation of protective lymphoid follicles within TB granulomas. Thus, we demonstrate a previously undescribed early protective role for ILCs in immunity to *Mtb* infection.

ILCs share features with both adaptive and innate immune cells and comprise of three main ILC subsets[2-5]. Type 1 ILCs produce IFN-γ and include NK cells and non-cytotoxic, non-NK type 1 ILCs[2-5]. Group 2 ILCs, which produce IL-4, IL-5 and IL-13, are involved in inflammatory-linked airway hyperactivity, tissue repair and helminth clearance[2-5]. Group 3 ILCs (ILC3) produce IL-17 and/or IL-22[6-8], and participate in the strategic positioning of immune cells in ectopic lymphoid structures[9]. Circulating ILC3s are enriched for uni- and multi-potent ILC precursors, and can give rise to all known ILC subsets, including NK cells in vivo[10]. ILCs are crucial for lung tissue repair following infection[11,12], and in generating hepatic granulomas[13]. Thus, we investigated the role of ILCs in the immune responses to TB. Using a validated flow cytometry panel (**Extended Data Fig. 1**), we found blood ILCs were highly

depleted in TB-infected participants compared to control participants, including the $CD117^+$ ILC3 subset (**Fig. 1a**), but not NK cells (**Extended Data Fig. 2a**). ILC depletion was not exacerbated by drug resistance or HIV-coinfection (**Fig. 1a; Extended Data Fig. 2b**). Using paired samples from HIV^- participants, we found that ILC1s and ILC3s rebounded after treatment, but ILC2s remained depleted (**Fig. 1b**). Thus, in contrast to persistent HIV infection[14], circulating ILC1s and ILC3s were restored once *Mtb* infection was cleared, confirming bacteraemia in modulating ILC accumulation. Whether ILC2s recover at a later time-point remains to be tested. Depletion of blood ILCs during acute HIV is associated with cell death[14]. However, TB infection was not associated with significant changes to caspase-3 expression in ILCs (**Extended Data Fig. 2c**), but an increase in the anti-apoptotic marker B-cell lymphoma 2 (BCL2) (**Fig. 1c**). In addition, ILC2s showed a significant upregulation of CD25 (**Fig. 1d**), a marker of activation and pro-survival phenotype in T cells[15,16]. These data suggest that circulating ILCs respond to *Mtb* infection but are not lost from the blood due to cell death.

We next asked if ILCs accumulate in the lungs following *Mtb* infection using a mouse model. C57BL/6 (B6) mice infected with aerosolized *Mtb* showed rapid early accumulation of ILC3s, but not ILC1s, with later accumulation of ILC2 (**Fig. 2a, Extended Data Fig. 3**), and ILC3s increased as infection proceeded (**Fig. 2a**). Simililarly, $ROR\gamma t^{-GFP}$ expressing ILC3 subset also accumulated during *Mtb* infection (**Fig. 2b**). Importantly, accumulation of ILC3s coincided with accumulation of alveolar macrophages (AMs), and preceded the accumulation of monocytes and recruited macrophages in the lung (**Fig. 2c**) and *Mtb* control in the lung (**Fig. 2d**). To confirm these observations in humans, we next examined fresh lung tissue, surgically resected from TB-infected participants, and identified tissue resident ILCs using established markers (**Extended Data Figs. 1 and 4a**). Here, and in contrast to blood, all ILC subsets, including $NKp44^+$ and $NKp44^-$ ILC3 subpopulations, but not NK cells, were increased compared to healthy lung tissue margins from non-TB lung controls (**Fig. 2e; Extended Data Figs. 4b and 4c**). Notably, this was not affected by HIV co-infection (**Extended Data Fig. 4d**).

Together, our results show that while circulating ILCs are reduced during PTB, they are rapidly increased upon infection in mice and accumulate in the lungs of both mice and human *Mtb*-infected participants.

The chemokine CXCL13, is induced in murine and human lungs during TB infection[17,18,19], and recruits lymphocytes via CXCR5 to mediate their spatial organization within lymphoid structures called inducible Bronchus associated lymphoid structures (iBALT)[18,19]. Consistent with this, high levels of CXCL13 were detected in the plasma of participants with PTB, that reduced following TB treatment (**Fig. 2f**), irrespective of HIV co-infection (**Extended Data Fig. 4e**). Furthermore, CXCR5 expression on all human ILC subsets in the blood was increased (**Fig. 2g**), as well as CD103 (**Extended Data Fig. 4f**), a tissue-resident lymphocyte marker. Subsequently, we detected distinct populations of CXCR5-expressing ILC3s, and CD103-expressing ILC2 and ILC3s in human TB lung tissue (**Extended Data Fig. 4g**). Importantly, human and mouse ILCs migrated in response to CXCL13, in a CXCR5-dependent manner in mouse ILC3s(**Extended Data Fig. 4h,i**). Given the role of CXCR5 in iBALT formation, we hypothesized that ILC3s in particular would localize within iBALT-containing TB lung granulomas. In histological sections from human PTB-infected participants we confirmed the enrichment of RAR-related orphan receptor gamma (Rorγt$^+$) and CD3- or CD3$^-$ CD127$^+$ ILC3s but not CD3$^+$ Rorγt$^+$ (Th17 cells) within granuloma associated lymphoid follicles compared to the low numbers of CD3$^-$Rorγt$^+$ ILC3s in necrotic TB granulomas and non-TB influenza infected lung tissue (**Fig. 2h,i and Extended Data Fig. 5**). To examine ILC3 localization during TB latency (LTBI), we turned to the rhesus macaque model of *Mtb* infection[19]. In macaques with TB, CD3$^-$Rorγt$^+$ ILC3s localized significantly within the non-necrotic well-formed iBALT containing TB granulomas of macaques with LTBI, but not within necrotic granulomas in macaques with PTB (**Fig. 2h,i**). These data together show that the CXCL13/CXCR5 axis is involved in functional recruitment of ILC3s to the lung following *Mtb* infection, and in the localisation of ILC3s to iBALT associated granulomas but not necrotic TB lesions.

Next, to characterize human lung ILCs, we performed RNA-sequencing on ILC2s and ILC3s sorted from fresh resected lungs of TB-infected participants and two controls (Sorted based on **Extended Data Fig. 1**; Purity of sort demonstrated in **Extended Data Fig. 6**). Differential expression (DE) analysis of ILC2s (45 DE genes), involved ILC2 genes indicative of inflammatory signalling (*IL-13, IL1RL1*), tissue repair (Amphiregulin, *AREG*) (**Fig. 3a, Extended Data Table. 1**), and Zinc Finger and BTB Domain Containing 16 (*ZBTB16*)*, which is* expressed during ILC development[20]. Notably, ILC2s expressed *KIT*, usually associated with ILC3s, but previously demonstrated in a subset of ILC2s (Insert Moro et al. 2010). ILC3s upregulated 1438 genes (**Fig. 3a, Extended Data Table. 2**), including the *RORC* and Natural Cytotoxic Receptor 3 (*NCR3)* genes, and genes encoding pro-inflammatory cytokines (*IL1B,* Colony stimulating factor *(CSF)-3 and* Oncostatin M *(OSM*)) associated with pulmonary TB and innate cell recruitment [21-23]. Accordingly, 7 chemokine genes, including CXCL1 (KC) and CXCL5, central to neutrophil recruitment in pulmonary TB[21,24], and the monocyte chemo-attractants CXCL17 and CCL2 (MCP-1), were all upregulated (**Fig. 3b**). Next, we identified potential upstream regulators of these responses by pathway analysis (**Fig. 3c; Extended Data Tables. 3, 4**). The predicted top upstream drivers of the transcriptional profile observed in sorted ILC2 cells were *IL-17*, *IL-6*, *CSF-1* and C-type lectin domain family 7 member A (*CLEC7A)*, pathways implicated in PTB[25-28], and Vasoactive Intestinal Peptide (*VIP)*, that is known to be elevated during lung inflammation and interacts with the ILC2 marker Chemoattractant Receptor Homologous Molecule Expressed On T Helper Type 2 (CRTH2)[29]. As VIP had not been directly linked to TB, we confirmed protein expression at in TB-infected human lung tissue using multiplexed fluorescent immunohistology (**Fig. 3d**). Top predicted upstream drivers of ILC3 responses are Interferon (*IFN)−γ*, *IL-1β,* Peroxisome proliferator-activated receptor *(PPAR)-γ* and Hepatocyte Nuclear Factor (*HNF) 4*, all previously characterized in the TB immune response[25,30,31], and OSM. The latter is less well studied in TB infection but, is detected in human granuolma[32], and can been seen in lung tissue sections examined in this study (**Fig. 3e**). Thus, 9/10 predicted upstream drivers of ILC transcription in

TB-infected lungs have known roles in TB infection and/or lung inflammation. Construction of gene interaction networks between our DE genes, and other published gene interactions, suggest that OSM may be linked to other major inflammatory cytokines, and inducers of cell growth and proliferation (**Fig. 3f, Extended Data Table. 5)**. Moreover, genes downstream of OSM encompassed key immune response pathways, including IFN-signaling, IL-6/STAT, and chemotaxis. Lastly, looking across all DE genes in ILC3s for enriched pathways describing ILC3 responses (**Fig. 3g, Extended Data Table. 6**), highlights IL-17 signaling. Taken together these first transcriptional data from human TB-infected lung ILCs, show a clear response to infection, and in particular support a role of ILC3s in coordinating lung immunity.

To address the mechanistic role of ILCs during *Mtb* infection, control mice, *Rag1*$^{-/-}$ and R*ag2* common gamma chain double knockout (*Rag2γc*$^{-/-}$) were aerosol infected with *Mtb* and early immune control was determined before accumulation of adaptive T cell responses occurred [33]. While *Rag1*$^{-/-}$ mice maintained early innate *Mtb* control similar to wild type mice at 14 days post infection (dpi), *Rag2γc*$^{-/-}$ mice exhibited increased *Mtb* CFU, and this coincided with absence of all lung ILC subsets (**Fig. 4a-b**). Importantly, increased early *Mtb* CFU in *Rag2γc*$^{-/-}$ could be rescued by adoptive transfer of sorted lung ILCs from *Mtb*-infected control mice (**Fig. 4a, Extended Data Fig. 7**). These results suggest that innate responses in *Rag1*$^{-/-}$ mice are sufficient to mediate early *Mtb* control provided common-γ chain-dependent ILCs are present. Furthermore, while *IFNγ*$^{-/-}$ and *IL-13*$^{-/-}$ mice maintained *Mtb* control at 14 dpi (**Extended Data Fig. 8a**), *Rorγt*$^{-/-}$ mice exhibited increased early *Mtb* lung burden (**Extended Data Fig. 8c**). The increased *Mtb* burden in *Rorγt*$^{-/-}$ mice coincided with decreased ILC3s accumulation (**Extended Data Fig. 8d**), while no changes in any ILCs were observed in *IFNγ*$^{-/-}$ and *IL-13*$^{-/-}$ mice (**Extended Data Fig. 8b**). These results were further confirmed by use of mice with specific deletion of ILC3s, namely *Ahr*$^{f/f}$ *Rorγt*^{Cre} mice, which exhibited increased early and late *Mtb* burden, decreased ILC3 and NKp46^{+} ILC3 accumulation and decreased alvelolar macrophage (AM) numbers in the lung, when compared to *Ahr*$^{f/f}$ *Mtb*-infected mice (**Fig. 4e,f**). ILC1s and ILC2s accumulation were comparable between *Ahr*$^{f/f}$*Rorγt*^{Cre} and *Ahr*$^{f/f}$ *Mtb*-infected

mice (**Fig. 4f**). This was corroborated in Core-Binding Factor Beta Subunit (*Cbfb)*$^{f/f}$*NKp46*^{Cre} mice, in which NKp46^{+} cells, including ILC1s, ILC3s and NK cells, are specifically depleted[34], and in whom *Mtb* infection led to drastically reduced lung ILC subset accumulation when compared with *Mtb*-infected *Cbfb*$^{f/f}$ mice (**Extended Data Fig. 9b**). Again, this coincided with reduced AM accumulation and resulted in increased early and late susceptibility to *Mtb* infection (**Extended Data Fig. 9a,b**). Complete depletion of NK cells (**Extended Data Fig. 10a**) did not impact *Mtb* control (**Extended Data Fig. 10b**). Additionally, baseline characterization of myeloid and lymphocytic population in lungs of *Ahr*$^{f/f}$*Ror*γ*t*^{Cre} and *Cbfb*$^{f/f}$*NKp46*^{Cre} mice were comparable (**Extended Data Fig. 9d,e and 11a,b**). Lung ILC3s produce IL-17 and IL-22 in response to IL-23 stimulation[4,7,35]. Murine lung cells infected with *Mtb* produced IL-23 (**Fig. 4g**). Moreover, lung cells infected with *Mtb* produced IL-22 and IL-17 when treated with recombinant IL-23 and IL-1β (**Fig. 4h**). Therefore, we next explored this axis and found *IL-17/IL-22*$^{-/-}$ mice displayed a significant early increase in lung *Mtb* burden (**Fig. 4i**), decreased number of lung ILC3s as well as CXCR5^{+} ILC3s, and decreased expression of CXCL13 mRNA expression within the granulomas (**Fig. 4j,k**). Accordingly, *in vivo* early neutralization of IL-23 in B6 mice resulted in reduced accumulation of early lung ILC3s (**Fig. 4m**), and increased early *Mtb* burden, when compared with isotype control treated B6 mice (**Fig. 4l**). Importantly, these early innate changes resulted in decreased formation of iBALT structures in all models (*Ahr*$^{f/f}$*Ror*γ*t*^{Cre}, *Cbfb*$^{f/f}$*NKp46*^{Cre}, *IL-22/IL-17*$^{-/-}$ and IL-23 depleted *Mtb*-infected mice), when compared with their respective controls (**Fig. 4n and Extended Data Fig. 9c**). Similarly, *CXCR5*$^{-/-}$ mice also exhibited increased lung *Mtb* CFU and decreased accumulation of ILC3s within lymphoid follicles, as well as decreased formation of iBALT structures (**Extended Data Fig. 12a-c**). Taken together, these data support an unexpected protective role for ILC3s in regulating early *Mtb* control through the production of IL-17 and IL-22 and formation of iBALT structures in a CXCR5-dependent manner.

Here we show that circulating ILCs are activated and recruited to the lung during human TB infection. Direct transcriptome sequencing of ILCs from fresh human tissue

revealed a co-ordinated response to infection. These data, therefore, support the unexpected participation of ILCs in the human immune response to TB. Crucially, we demonstrate the importance of ILC3s to the outcome of infection using multiple mouse models, showing that a reduction in lung ILC3s impaired early immune control of *Mtb*. The associated increase in lung bacterial burden coincided with decreased IL-17 and IL-22 production, compromised AM accumulation, and impaired iBALT organization which was dependent on the CXCR5 and CXCL13 axis; key aspects of the immune response to *Mtb*. Taken together, our finding for the first time show that ILCs respond to *Mtb* infection and play an important role in determining the outcome of disease during TB.

Acknowledgements

This work was supported by Washington University in St. Louis, NIH grant HL105427, AI111914-02 and AI 123780 to SAK and DK, AI134236-02 to SAK, MC and DK, and NIH/NHLBI T32 HL007317-37 to RDG. Department of Molecular Microbiology, Washington University St Louis, and Stephen I. Morse Fellowship to S.D, T32 HL 7317-39 to N.H and T32-AI007172 to M.D. JRM was supported by funds of the Department of Medicine, University of Rochester, and NIH grant U19 AI91036. The authors thank Amgen for providing anti IL-23 antibody for the study. The authors thank Dr. Jennifer Bando for helping with the flow cytometry. The authors thank Dr. Michael Holtzman for generously gifting IL-13$^{-/-}$ mice.

METHODS

Participants

TB-infected blood and plasma samples were obtained from the collection of urine, blood and sputum (CUBS) cohort, based at Prince Cyril Zulu communicable disease centre and the Nelson R. Mandela School of Medicine. Fifty blood samples were taken, from participants with confirmed pulmonary TB (Gene Xpert, sputum smears or culture method), of which 27 were HIV co-infected and 23 were HIV negative. Control blood samples (TB^{-}HIV^{-}) were collected

from the Females Rising through Empowerment, Support and Health (FRESH) cohort from Umlazi, Durban.

TB affected lung tissue samples were obtained from 33 participants undergoing surgical resections due to severe lung complications, including haemoptysis, bronchiectasis, persistent cavitatory disease, shrunken or collapsed lung or drug-resistant infection, at the King Dinuzulu hospital in Durban, KwaZulu-Natal and Inkosi Albert Luthuli Central Hospital (IALCH) in Durban, KwaZulu-Natal. 6 TB^- control samples with macroscopically normal tissue margins from lung cancer resections or other inflammatory lung diseases from IALCH in Durban, KwaZulu-Natal were included in the study.

For some histological studies, lung sections were obtained from parcipants with TB and LTBI from the Tuberculosis Outpatient Clinic at the National Institute of Respiratory Diseases (INER) in Mexico City. Samples were obtained from participants prior to anti-*Mtb* treatment.

All participants provided informed consent and each study was approved by the respective institutional review boards including the Biomedical Research Ethics Committee of the University of KwaZulu-Natal or INER.

Sample preparation

Blood samples were processed from frozen PBMCs purified using standard ficoll separation. Samples were thawed in DNase-containing (25 units/ml) R10 (Sigma) at 37°C. Cells were rinsed and rested at 37°C for a minimum of one hour before undergoing red blood cell lysis by 5-10ml RBC lysis solution (Qiagen) for 20 minutes at room temperature. Cells were then stained with the appropriate antibody panel described below.

Blood for plasma isolation was centrifuged at 200 rpm for 10 minutes. The plasma layer was removed, frozen down in 1ml aliquots and stored at -80°C until needed. Later these samples were thawed at room temperature and vortexed thoroughly before usage.

Lung samples were processed from fresh tissue immediately following surgery. Resected tissues were washed with cold HBSS (Sigma) and dissected into smaller pieces. Tissues were rinsed again and resuspended in 10ml R10, containing DNAse (1µl/ml) and Collagenase (4µl/ml), and disassociated in a Gentle MACS dissociator (Miltenyi Biotec). Cells were rested in a shaking incubator at 37°C for 30 minutes and then further processed in the gentle MACS dissociator. After further resting (30 mins at 37°C) and washing steps, cells were strained through a 70µm cell strainer and washed one final time. Cells were lysed using 5-10 ml RBC lysis buffer (Qiagen) and stained for flow cytometry analysis.

Mtb infection in mice

C57BL/6 (B6), *IFN-$\gamma^{-/-}$, Rag1$^{-/-}$, CXCR5$^{-/-}$, Rag2γc$^{-/-}$, Rorγt$^{-/-}$, Rorc(γt)-EGFP* mice were obtained from Jackson Laboratory (Bar Harbor, ME) and bred at Washington University in St. Louis. *IL-17$^{-/-}$*[36] and *IL-22$^{-/-}$*[37] mice were crossed at Washington University in St. Louis to obtain double knockout mice. *Cbfb*$^{f/f}$, *Cbfb$^{f/f}$NKp46^{Cre}*[34] breeder pairs were a generous gift from Dr. Wayne Yokoyama. *IL-13$^{-/-}$* breeder pairs were a generous gift from Dr. Michael Holtzman. *Ahr$^{f/f}$, Ahr$^{f/f}$Rorγt^{Cre}* mice were generously provided by Dr. Marco Colonna. Experimental mice were age and sex-matched and used between 6-8 weeks of age. *Mtb* W. Beijing strain, HN878, was cultured to mid-log phase in Proskauer Beck medium containing 0.05% Tween 80 and frozen in 1ml aliquots at -80°C. Mice were infected with aerosolized ~100 CFU of bacteria using a Glas-Col airborne infection system. Lungs were harvested, homogenized and serial dilutions of tissue homogenates were plated on 7H11 plates and CFU counted. Anti-IL-23p19 (Amgen, 16E5, 500 µg per mouse) and mouse IgG1 isotype (500 µg per mouse) were generously provided by Amgen and intraperitoneally (i.p.) injected into B6 mice one day prior to infection. Anti-NK1.1 (PK136, 100 µg per mouse) and mouse IgG2a isotype (100 µg per mouse) were kindly provided by Dr. Wayne Yokoyama and injected i.p. on day 0 and every 3 days post-infection.

Flow cytometry

Blood and lung tissue human ILCs were identified by a surface stain that included a near-infrared live/dead cell viability cell staining kit (Invitrogen) and the following monoclonal antibodies: CRTH2 (clone BM16, BD Biosciences), CD127 (clone R34.34, Beckman Coulter), CD117 (clone 104D2, BioLegend), CD56 (clone HCD56, BioLegend), CD25 (clone BC96, BioLegend), CD94 (clone HP-3D9, BD Biosciences), CD161 (clone HP-3G10, BioLegend), NKp44 (clone Z231, Beckman Coulter), CD16 (clone 3G8, BioLegend), CD4 (clone RPA-T4, BD Biosciences), and CD45 (clone HI30, BD Biosciences). Lineage markers CD19 (clone HIB19, BD Biosciences), CD34 (clone 561, BioLegend), CD14 (clone HCD14, BioLegend), CD4 (clone OKT4, BioLegend), TCR$\alpha\beta$ (clone IP26, BioLegend), TCR$\gamma\delta$ (clone B1, BioLegend), BDCA2 (clone 201A, BioLegend) and FcER1 (clone AER-37 (CRA1), eBioscience). Intracellular stains were done following Fix/Perm kit (BD Biosciences) and included CD3 (clone UCHT1, BD Biosciences) and CD3 (clone HIT3A, BD Biosciences).

Modified antibody panels were used to stain for markers of apoptosis or lung-homing. These panels consisted of a near-infrared live/dead cell viability cell staining kit (Invitrogen) and the following monoclonal antibodies: CD117 (clone 104D2, Biolegend), CD45 (clone HI30, BD Biosciences), CD161 (clone HP-3G10, BioLegend), CD56 (clone HCD56, BioLegend), CD94 (clone HP3D9, BD Bioscience), CD127 (clone R34.34, Beckman Coulter), CRTH2 (clone BM16, BD Biosciences), CD19 (SJ25C1, BD Bioscience), CD3 (OKT3, Biolegend) or CD69 (clone FNSO, BioLegend), CD4 (clone RPA-T4, BD Bioscience), CXCR3 (clone 1C6, BD Bioscience) or CD3 (clone UCHT1, BD Biosciences), CXCR5 (clone RF8B2, BD Bioscience) and CD103 (clone Ber-ACT8, Biolegend). Intracellular stains were done following Fix/Perm kit (BD Biosciences) and included Caspase-3 (clone C92-605, BD Bioscience) and BCL2 (clone 100, BD Bioscience).

Cells were surface stained with 25µl of the appropriate antibody panel at room temperature in the dark, for 20 minutes. Following the BD Bioscience Fix/Perm step, cells were stained with the corresponding intracellular panel for a minimum of 20 minutes in the dark before being fixed with 2% paraformaldehyde. Fixed cells were acquired on a 4 laser BD Fortessa flow

cytometer (CUBS and fresh blood samples) or a 5 laser FACSARIA Fusion (Lung, chemokine and apoptosis experiment samples) within 24 hours of processing. All flow cytometry data were analysed using FlowJo version 9.7.6 (TreeStar).

Murine lung cell isolation and preparation were performed as described previously[38]. Briefly, mice were asphyxiated with CO_2 and lungs were perfused with heparin in saline. Lungs were minced and incubated in collagenase/dnase (Sigma) for 30 minutes at 37°C. Lungs were pushed through a 70µm nylon screen to release cells. Following red blood cell lysis, cells were used for flow cytometric analysis. The following antibodies were from TonBo Biosciences (San Diego, CA, USA): CD127 (clone A7R34), CD3 (clone 145-2C11), CD19 (clone 1D3). Antibodies purchased from eBioscience (San Diego, CA, USA) were:, RORc(γt) (clone AFKJS-9), , Sca-I (clone D7). CD45 (clone 30-F11), CCR6 (clone 140706), IL-17 (TC11-18H10), Streptavidin and CXCR5 (clone 2G8) were purchased from Becton Dickinson (Franklin Lakes, NJ, USA). The following antibodies were from Invitrogen (Carlsbad, CA, USA): Biotinylated NKp46, TER-119 (clone TER-119), CD11c (clone N418), IL-22 (clone 1H8PWSR) and CD5 (clone 53-7.3).Live-dead aqua was purchased from Thermo Fisher Scientific (CA, USA). For intracellular staining, fixation/permeabilization concentrate and diluent (eBioscience) were used to fix and permeabilize lung cells for 20mins. The cells were incubated overnight with the intracellular staining. Samples were run on 4 laser BD Fortessa flow cytometer.

Adoptive transfer

Total ILCs (excluding ILC1, $CD45^+CD127^+Lin^-NK1.1^-$) were purified on a FACSJazz machine from the lungs of *Mtb* infected B6 mice following enrichment with CD45 and staining with the above mentioned antibodies. About 5000 sorted and highly purified ILCs were intratracheally transferred into the *Rag2*$\gamma c^{-/-}$ mice.

ELISA

The Quantikine ELISA assay for human CXCL/13/BLC/BCA-1 was used to measure the amount of CXCL13 in the plasma of 19 participants before and after 6 months of successful TB treatment. Standards, controls and samples were run in triplicate. Results were measured at 450nm using the GlowMax- Multi detection system (Promega). Concentrations were determined based on the standard curve generated on GraphPad prism version 6.0 (GraphPad Software, Inc.). Protein levels for mouse cytokines (IL-17, IL-22 and IL-23) in culture supernatants were measured using mouse ELISA kits or multiplex according to manufacturer's instruction (R&D Systems, MBL International Corporation, Woburn, MA).

In vitro chemotaxis assays

10000 human ILCs were sorted in duplicate (1 control and 1 experiment per individual) from PBMCs by using the FACS panel described above, on a 5-laser FACSARIA Fusion. Cells were directly sorted into 100 µL of freshly prepared media (HBSS containing 10% FBS) at 4ºC and transferred into the top well of a Corning HTS 24-well transwell plate. Bottom chambers of transwell plates were loaded with 600 µL of either media alone, for controls, or media and 500 ng/mL of recombinant human CXCL13 (R&D Systems) for experimental wells. Transwell plates were incubated for 2h and then aspirate from bottom chamber was mixed with 50 µL of precision count beads (BioLegend) and acquired on a FACSARIA Fusion. As antibody stains from intial sort remained visible, ILC3s were identified and then counted using counting beads as per manufacturers instruction.

For mouse chemotaxis assay, mouse ILCs (excluding ILC1, $CD45^{+}CD127^{+}$ $Lin^{-}NK1.1^{-}$) were sorted from *Mtb*-infected B6 mice after CD45 enrichment within the total lung cells using the staining panel described above, on a FACSJAZZ machine. Cells were directly sorted into 100 µL of freshly prepared media (HBSS containing 10% FBS) at 4ºC and transferred into the top well of a Corning HTS 24-well transwell plate. Bottom chambers of transwell plates were loaded with 600 µL of either media alone, for controls, or media and 500 ng/mL of recombinant

mouse CXCL13 (R&D Systems) for experimental wells. Transwell plates were incubated for 2h and then aspirate from bottom chamber was stained using the ILC3 marker panel on 4 laser BD Fortessa flow cytometer to determine the exact number of ILC3 migrating towards the CXCL13 gradient.

Multiplex Fluorescent Immunohistology

Fluorescent immunohistology was either performed on histological sections of TB-infected lung tissues that were either supplied by Dr Pratista Ramdial of IALCH or prepared in-house from formalin-fixed lung tissue following resections. Sections were dried overnight at 60ºC and then processed using an Opal 4-colour Manual IHC kit (Perkin Elmer) as per manufacturer's instructions with CD20 (1:400), CD3 (1:400) and CD127 (1:100), VIP (1:100) and OSM (1:100) as primary antibodies. Slides were scanned on a Zeiss Axio Observer microscope using TissueFAXS imaging software (Tissuegnostics) and analysed using TissueQuest analysis software (Tissuegnostics).

Whole Transcriptome Amplification and RNA Sequencing

ILC2 and ILC3 populations were sorted from lung tissue from 5 TB-infected and 2 cancer control participants using a 5 laser FACSARIA Fusion. A validated 17-colour FACS panel (**Extended Data Fig. 1**), and stringent gating was used to identify ILC2 and ILC3 populations in these samples. Cells were directly sorted into RLT buffer (Qigen) + 1% β-Mercaptoethanol. Lysates were snap frozen on dry ice and stored at -80°C. As input numbers were low (50-1385 cells), thawed lysate was split into three technical replicates for each sample to increase the probability of successful amplification. RNA extraction, cDNA conversion and whole transcriptome amplification was carried out as previously described using Smart-seq2[14]. Quality of the amplified product was confirmed using a high sensitivity DNA analysis kit and a 2100 BioAnalyzer (Aligent Technologies), and concentrations measured using a Qubit assay kit (ThermoFisher Scientific). Diluted samples were tagmented, amplified, and individually barcoded using a Nextera XT DNA Library prep kit (Illumina), cleaned using AMPure XP SPRI

beads (Beckman Coulter) and sequenced on a NextSeq 500 (Illumina) using 30x30 PE reads with 8x8 index reads to an average depth of $14.9x10^6$ reads.

mRNA expression

RNA was extracted from the sorted ILCs ($CD45^+CD127^+Lin^-NK1.1^-$) using the Qiagen RNeasy Mini kit (Qiagen). cDNA was generated using ABI reverse transcription reagents (ABI, ThermoFisher) and RT-PCR was run on a Viia7 Real-Time PCR system (Life Technologies, Thermo Fisher). The relative expression of Ccr6, Rorc, and Ahr in sorted ILCs was calculated over expression of GAPDH in each sample. The primer and probe sequences for murine glyceraldehyde 3-phosphate dehydrogenase (GAPDH) were previously published[39]. The primer and probes for murine *Ccr6*, *Rorc*, and *Ahr* were purchased from Applied Biosystems.

RNA-Seq Data Analysis

Sequencing data from the NextSeq 500 was demultiplexed and aligned against hg38 using TopHat[40], and expression values, in counts, were generated in RSEM[41] for every sample. Samples with fewer than 10^6 aligned transcriptionally reads, or fewer than 10,000 measured genes, and genes expressed with fewer than 5 counts in fewer than 4 samples were discarded from subsequent analysis.

Differential expression analysis was performed in R (build 3.3.2) using the DESeq2 package[42] (version 1.14.1) on ILC2s and ILC3s between samples (and replicates) from 5 TB positive and 2 TB negative individuals. The DESeq2 results can be found in **Extended DataTables 1 and 2**; hits with FDR < 0.01 were considered differentially expressed for downstream analyses. DE genes and their significances and log fold changes for each comparison were then processed using Ingenuity Pathway Analysis (QIAGEN INC., https://www.qiagenbioinformatics.com/products/ingenuity-pathway-analysis) to populate lists of predicted upstream drivers (**Extended DataTables 3 and 4**). Upstream driver plots were generated from the "Upstream Analysis" on IPA; hits with 'Molecule Type' including the word "chemical", '*p*-value of overlap' > 0.01, and number of 'Target molecules in dataset' < 3 were

412 excluded from plotting. OSM upstream driver network was created using the Mechanistic
413 Networks generated by IPA, using a *p*-value< 0.01 for overlap significance. The downstream
414 driver network for genes known to interact with OSM was generated using the ClueGO plugin[43]
415 (version 2.3.3) in Cytoscape (version 3.3.0) with following ontologies: GO Biological Process,
416 GO Immune System Process, KEGG, and REACTOME Pathways. Only pathways with
417 significance of $p < 0.01$ after Benjamaini-Hochberg correction were shown, and a Kappa Score
418 Threshold of 0.45 was used to merge terms. The downstream pathway bar chart was
419 generated from the "Downstream Pathways" on IPA where large categories were manually
420 annotated.

421 **ILC3 staining and quantification**

422 Immunohistochemical staining of human, non-human primate and mouse formalin-fixed
423 paraffin-embedded lung sections were initially dewaxed in xylene prior to hydrating with
424 decreasing graded alcohol and methanol passages. Antigen was retrieved via heat treatment
425 in 92°C and EDTA buffer pH 8. Tissue staining with RORγt (Clone 6F3.1, Millipore for mouse;
426 clone Q31-378, BD Bioscience for NHP and human), CD3 (clone SP7, Thermofisher for
427 human, NHP and mouse) or PAX5 (Clone 24/Pax-5, BD Pharmingen, for human and NHP)
428 or B220 antibody (clone RA3-6B2, BD Pharmingen) was performed for one hour in a humid
429 chamber. Tissues were washed in Tris buffered saline pH7.4-7.6 prior to incubation with
430 secondary antibody (Novocastra Post Primary, Leica) and polymer (Novolink Polymer, Leica).
431 To develop the reaction, tissues were incubated with 3,3'-Diaminobenzidine chromogen (DAB,
432 Leica). Singly stained sections (PAX5, B220) were incubated with DAB for 5 min and tissues
433 receiving double staining (RORγt and CD3) were incubated overnight. Tissues were
434 counterstained with haematoxylin and rinsed in water. All tissues were mounted with
435 coverslips using glycerol mounting medium. $CD3^{-}ROR\gamma t^{+}$ ILC3 were quantified in the slides.
436 Images were analyzed manually by counting the number of ILC3 cells per field. The analysis
437 was done in a blinded manner.

438 **Immunofluorescence staining and In situ Hybridization**

Mouse lung lobes were perfused with 10% formalin, fixed and paraffin embedded. Briefly, the Formalin-fixed paraffin-embedded sections were processed to remove paraffin and then hydrated in 96% alcohol and phosphate-buffered saline. Antigens were retrieved with a DakoCytomation Target Retrieval Solution (Dako, Carpinteria, CA, USA), and non-specific binding was blocked by using 5% (v/v) normal donkey serum and Fc block (BD Pharmingen). Sections were then probed with anti-B220 and anti-CD3 (clone M-20, Santa Cruz Biotechnology, Santa Cruz, CA; dilution: 1/100) to detect B cell follicle formation (clone RA3-6B2, BD Pharmingen; dilution: 1/100). For B-cell follicles analyses, follicles were outlined with the automated tool of the Zeiss Axioplan 2 microscope (Zeiss, Thornwood, NY, USA), and total area and average size was calculated in squared microns.

To detect $CD3^{-}Ror\gamma t^{+}$ ILC3s and $CD20^{+}$ B cells in lungs of NHP and humans infected with TB, slides were incubated with primary goat anti-CD3-epsilon (clone M-20, Santa Cruz Biotechnology), mouse anti-human Rorγt (clone 6F3.1, Milipore Sigma) and rabbit anti-human CD20 (LS-B2605-125, Lifespan Biosciences). To detect $CD3^{-}Ror\gamma t^{+}$ ILC3s and $CD20^{+}$ B cells in mice lungs infected with TB, slides were incubated with primary goat anti-CD3-epsilon (clone M-20, Santa Cruz Biotechnology), monoclonal rabbit anti-mouse Rorγt (clone EPR20006, Abcam) and APC-rat anti-mouse CD45R (B220, cloneRA3-6B2, BD Biosciences).Slides were incubated with primary antibodies overnight, at room temperature in a humid chamber. Next day, slides were briefly washed in PBS, and primary antibodies were revealed with Alexa Fluor 568 donkey anti-goat Ig G (A11057, Thermo Fisher Scientific), FITC-donkey anti-mouse Ig G (715-095-150, Jackson ImmunoResearch Laboratories), biotin-donkey anti-rabbit (711-065-162, Jackson ImmunoResearch Laboratories) or Alexa Fluor 568 donkey anti-goat Ig G (A11057, Thermo Fisher Scientific) and Alexa Fluor 488-donkey anti-rabbit Ig G (711-546-152, Jackson ImmunoResearch Laboratories) for human/NHP slides or mouse slides respectively. Finally, streptavidin Alexa Fluor 680 (S32358, Thermo Fisher Scientific) was added to the slides to visualize CD20) for human/NHP sections. Slides were washed in PBS and mounted with Vectashield antifade mounting media with DAPI (Vector

Laboratories, H-1200). ILC3 were counted in 3-5 random 200x fields in each individual slide. 200x representative pictures were taken with Axioplan Zeiss Microscope and recorded with a Hamamatsu camera.

FFPE lung sections were subjected to in situ hybridization (ISH) with the mouse-CXCL13 probe using the RNAscope 2.5HD Detection Kit (Brown staining) as per the manufacturer's instruction (Advanced Cell Diagnostics, Newark, CA). The representative pictures were captured with the Hamamatsu Nanozoomer 2.0 HT system with NDP scan image acquisition software. The CXCL13 positive and total area per lobe was quantified in a 40x magnification. Ratio was calculated by dividing CXCL13 positive area by total area on each lobe.

Statistical Analyses

Where MFI data were measured at different time points, MFI was converted to final relative MFI by normalizing each measurement by an internal control to standardize these measurements over time[44]. The Mann-Whitney *U* test was used to determine statistical significance between two groups only while significance between more than two groups was calculated using the Dunn's multiple comparisons test or a Mann-Whitney U test with Bonferroni corrections. Comparisons between matched samples where data were paired were analysed with the Wilcoxon matched-pairs signed rank test. All statistical analyses were performed using GraphPad Prism version 6.0d (GraphPad Software, Inc.)

In mouse studies, differences between the means of two groups were analyzed using two-tailed student's *t*-test in Prism 5 (GraphPad, La Jolla, CA, USA). Differences between the means of three or more groups were analyzed using One-way ANOVA with Tukey's post-test. A *p*-value of <0.05 was considered significant.

REFERENCES

1 Organization, W. H. Global tuberculosis report 2014. (2014).

2 Price, A. E. *et al.* Systemically dispersed innate IL-13-expressing cells in type 2 immunity. *Proc Natl Acad Sci U S A* **107**, 11489-11494, doi:10.1073/pnas.1003988107 (2010).

3 Eberl, G., Colonna, M., Di Santo, J. P. & McKenzie, A. N. Innate lymphoid cells. Innate lymphoid cells: a new paradigm in immunology. *Science* **348**, aaa6566, doi:10.1126/science.aaa6566 (2015).

4 Klose, C. S. & Artis, D. Innate lymphoid cells as regulators of immunity, inflammation and tissue homeostasis. *Nat Immunol* **17**, 765-774, doi:10.1038/ni.3489 (2016).

5 Diefenbach, A., Colonna, M. & Koyasu, S. Development, differentiation, and diversity of innate lymphoid cells. *Immunity* **41**, 354-365, doi:10.1016/j.immuni.2014.09.005 (2014).

6 Hue, S. *et al.* Interleukin-23 drives innate and T cell-mediated intestinal inflammation. *J Exp Med* **203**, 2473-2483, doi:10.1084/jem.20061099 (2006).

7 Satoh-Takayama, N. *et al.* Microbial flora drives interleukin 22 production in intestinal NKp46+ cells that provide innate mucosal immune defense. *Immunity* **29**, 958-970, doi:10.1016/j.immuni.2008.11.001 (2008).

8 Takatori, H. *et al.* Lymphoid tissue inducer-like cells are an innate source of IL-17 and IL-22. *J Exp Med* **206**, 35-41, doi:10.1084/jem.20072713 (2009).

9 Scandella, E. *et al.* Restoration of lymphoid organ integrity through the interaction of lymphoid tissue-inducer cells with stroma of the T cell zone. *Nat Immunol* **9**, 667-675, doi:10.1038/ni.1605 (2008).

10 Lim, A. I. *et al.* Systemic Human ILC Precursors Provide a Substrate for Tissue ILC Differentiation. *Cell* **168**, 1086-1100 e1010, doi:10.1016/j.cell.2017.02.021 (2017).

11 Monticelli, L. A. *et al.* Innate lymphoid cells promote lung-tissue homeostasis after infection with influenza virus. *Nature Immunology* **12**, 1045-1054, doi:10.1038/ni.2131 (2011).

12 Kim, H. Y., Umetsu, D. T. & Dekruyff, R. H. Innate lymphoid cells in asthma: Will they take your breath away? *Eur J Immunol* **46**, 795-806, doi:10.1002/eji.201444557 (2016).

13 McHedlidze, T. *et al.* Interleukin-33-dependent innate lymphoid cells mediate hepatic fibrosis. *Immunity* **39**, 357-371, doi:10.1016/j.immuni.2013.07.018 (2013).

14 Kloverpris, H. N. *et al.* Innate Lymphoid Cells Are Depleted Irreversibly during Acute HIV-1 Infection in the Absence of Viral Suppression. *Immunity* **44**, 391-405, doi:10.1016/j.immuni.2016.01.006 (2016).

15 Hedfors, I. A. & Brinchmann, J. E. Long-term proliferation and survival of *in vitro*-activated T cells is dependent on interleukin-2 receptor signalling but not on the high-affinity IL-2R. *Scandinavian Journal of Immunology* **58**, 522-532 (2003).

16 Ladanyi, A. *et al.* T-cell activation marker expression on tumor-infoltrating lymphocytes as prognostic factor in cutaneous malignant melanoma. *Clinical Cancer Research* **10**, 521-530 (2004).

17 Kang, D. D., Lin, Y., Moreno, J. R., Randall, T. D. & Khader, S. A. Profiling early lung immune responses in the mouse model of tuberculosis. *PLoS One* **6**, e16161, doi:10.1371/journal.pone.0016161 (2011).

18 Khader, S. A. *et al.* In a murine tuberculosis model, the absence of homeostatic chemokines delays granuloma formation and protective immunity. *J Immunol* **183**, 8004-8014, doi:10.4049/jimmunol.0901937 (2009).

19 Slight, S. R. *et al.* CXCR5(+) T helper cells mediate protective immunity against tuberculosis. *J Clin Invest* **123**, 712-726, doi:10.1172/JCI65728 (2013).

20 Constantinides, M. G., McDonald, B. D., Verhoef, P. A. & Bendelac, A. A committed precursor to innate lymphoid cells. *Nature* **508**, 397-401, doi:10.1038/nature13047 (2014).

21 Dorhoi, A. *et al.* The adaptor molecule CARD9 is essential for tuberculosis control. *J Exp Med* **207**, 777-792, doi:10.1084/jem.20090067 (2010).

22 Traber, K. E. *et al.* Induction of STAT3-Dependent CXCL5 Expression and Neutrophil Recruitment by Oncostatin-M during Pneumonia. *Am J Respir Cell Mol Biol* **53**, 479-488, doi:10.1165/rcmb.2014-0342OC (2015).
23 Charmoy, M. *et al.* The Nlrp3 inflammasome, IL-1beta, and neutrophil recruitment are required for susceptibility to a nonhealing strain of Leishmania major in C57BL/6 mice. *Eur J Immunol* **46**, 897-911, doi:10.1002/eji.201546015 (2016).
24 Nouailles, G. *et al.* CXCL5-secreting pulmonary epithelial cells drive destructive neutrophilic inflammation in tuberculosis. *J Clin Invest* **124**, 1268-1282, doi:10.1172/JCI72030 (2014).
25 O'Garra, A. *et al.* The immune response in tuberculosis. *Annu Rev Immunol* **31**, 475-527, doi:10.1146/annurev-immunol-032712-095939 (2013).
26 Pagan, A. J. *et al.* Myeloid Growth Factors Promote Resistance to Mycobacterial Infection by Curtailing Granuloma Necrosis through Macrophage Replenishment. *Cell Host Microbe* **18**, 15-26, doi:10.1016/j.chom.2015.06.008 (2015).
27 van de Veerdonk, F. L. *et al.* Mycobacterium tuberculosis induces IL-17A responses through TLR4 and dectin-1 and is critically dependent on endogenous IL-1. *J Leukoc Biol* **88**, 227-232, doi:10.1189/jlb.0809550 (2010).
28 Yadav, M. & Schorey, J. S. The beta-glucan receptor dectin-1 functions together with TLR2 to mediate macrophage activation by mycobacteria. *Blood* **108**, 3168-3175, doi:10.1182/blood-2006-05-024406 (2006).
29 El-Shazly, A. E. *et al.* Novel association between vasoactive intestinal peptide and CRTH2 receptor in recruiting eosinophils: a possible biochemical mechanism for allergic eosinophilic inflammation of the airways. *J Biol Chem* **288**, 1374-1384, doi:10.1074/jbc.M112.422675 (2013).
30 Rajaram, M. V. *et al.* Mycobacterium tuberculosis activates human macrophage peroxisome proliferator-activated receptor gamma linking mannose receptor recognition to regulation of immune responses. *J Immunol* **185**, 929-942, doi:10.4049/jimmunol.1000866 (2010).
31 Tientcheu, L. D. *et al.* Differential transcriptomic and metabolic profiles of M. africanum- and M. tuberculosis-infected patients after, but not before, drug treatment. *Genes Immun* **16**, 347-355, doi:10.1038/gene.2015.21 (2015).
32 O'Kane, C. M., Elkington, P. T. & Friedland, J. S. Monocyte-dependent oncostatin M and TNF-alpha synergize to stimulate unopposed matrix metalloproteinase-1/3 secretion from human lung fibroblasts in tuberculosis. *Eur J Immunol* **38**, 1321-1330, doi:10.1002/eji.200737855 (2008).
33 Khader, S. A. *et al.* IL-23 and IL-17 in the establishment of protective pulmonary CD4+ T cell responses after vaccination and during Mycobacterium tuberculosis challenge. *Nature Immunology* **8**, 369-377 (2007).
34 Ebihara, T. *et al.* Runx3 specifies lineage commitment of innate lymphoid cells. *Nat Immunol* **16**, 1124-1133, doi:10.1038/ni.3272 (2015).
35 Cupedo, T. *et al.* Human fetal lymphoid tissue-inducer cells are interleukin 17-producing precursors to RORC+ CD127+ natural killer-like cells. *Nat Immunol* **10**, 66-74, doi:10.1038/ni.1668 (2009).
36 Nakae, S. *et al.* Antigen-specific T cell sensitization is impaired in IL-17-deficient mice, causing suppression of allergic cellular and humoral responses. *Immunity* **17**, 375-387 (2002).
37 Aujla, S. J. *et al.* IL-22 mediates mucosal host defense against Gram-negative bacterial pneumonia. *Nat Med* **14**, 275-281, doi:10.1038/nm1710 (2008).
38 Domingo-Gonzalez, R. *et al.* Interleukin-17 limits hypoxia-inducible factor 1alpha and development of hypoxic granulomas during tuberculosis. *JCI Insight* **2**, doi:10.1172/jci.insight.92973 (2017).

588 39 Gopal, R. *et al.* Unexpected role for IL-17 in protective immunity against hypervirulent
589 Mycobacterium tuberculosis HN878 infection. *PLoS Pathog* **10**, e1004099,
590 doi:10.1371/journal.ppat.1004099 (2014).
591 40 Trapnell, C. *et al.* Differential gene and transcript expression analysis of RNA-seq
592 experiments with TopHat and Cufflinks. *Nat Protoc* **7**, 562-578, doi:10.1038/nprot.2012.016
593 (2012).
594 41 Li, B. D., C. N. RSEM: accurate transcript quantification from RNA-Seq data with or without a
595 reference genome. *BMC Bioinformatics* **12** (2011).
596 42 Love, M. I., Huber, W. & Anders, S. Moderated estimation of fold change and dispersion for
597 RNA-seq data with DESeq2. *Genome Biol* **15**, 550, doi:10.1186/s13059-014-0550-8 (2014).
598 43 Bindea, G. *et al.* ClueGO: a Cytoscape plug-in to decipher functionally grouped gene ontology
599 and pathway annotation networks. *Bioinformatics* **25**, 1091-1093,
600 doi:10.1093/bioinformatics/btp101 (2009).
601 44 Upreti, D., Pathak, A. & Kung, S. K. Development of a standardized flow cytometric method
602 to conduct longitudinal analyses of intracellular CD3zeta expression in patients with head
603 and neck cancer. *Oncol Lett* **11**, 2199-2206, doi:10.3892/ol.2016.4209 (2016).

604

Figure Legend

Figure 1. Circulating ILCs are depleted and activated in response to TB. (a) Circulating ILC subsets were enumerated in blood of HIV+ and HIV- TB participants, and healthy controls by flow cytometry. Significance by Kruskal-Wallis test with corrections for multiple comparisons. **(b)** Paired ILC subsets in the blood before and after standard TB treatment were compared to frequencies in healthy controls (*p*-value by Wilcoxon matched-pairs test). Pre-TRT = untreated; TRT = after treatment. **(c)** The median fluorescent intensity (MFI) of the anti-apoptotic marker BCL2 was measured in TB+ and control participants on all ILC subsets, and in $CD56^{hi}$ NK cells, but not $CD56^{dim}$ NKs, $CD4^{+}$, $CD4^{-}$ $CD3^{+}$ T cells and CD19-expressing B cells. Significance by unpaired Mann-Whitney U test with Bonferroni corrections. **(d)** Expression of activation and pro-survival marker CD25 was determined using flow cytometry in ILC subsets in blood from HIV+ and HIV- TB participants. Significance by Kruskal-Wallis test with corrections for multiple comparisons.

Figure 2. ILCs rapidly accumulate within lung tissues and are associated with structures of TB histopathology. **(a-c)** C57BL/6 (B6, n=5) mice or *Rorγt-eGFP* mice were aerosol infected with ~100 CFU *Mtb.* **(a)** Numbers of ILC1s, ILC2s, ILC3s in B6 mice and **(b)** number of ILC3s in *Rorγt-eGFP* mice were quantified by flow cytometric analyses. (**c**) Numbers of alveolar macrophages (AMs), monocytes, and recruited macrophages (RMs) were measured and quantified by flow cytometric analyses in B6 mice. **(d)** Bacterial burden was measured in the lungs of B6 mice by plating. Data shown as mean ± SEM (a) or mean ± SD (b-d). Where *p*-value not shown, **p*<0.05, ***p*<0.01, *****p*<0.0001. Significance by Student's *t*-test **(a-c)**. **(e)** Human ILC subsets were measured in TB infected lung tissue (TB^{+}) compared to TB^{-} control lung tissue, and in the circulation using flow cytometry. Significance by Kruskal-Wallis test with adjustments for multiple comparisons was carried out. **(f)** CXCL13 protein levels were measured in plasma from drug-susceptible TB subjects, and after 6 months of standard TB treatment (two-tailed Wilcoxon matched-pairs test). (**g**) CXCR5 expression was measured on circulating ILC subsets using flow cytometry. Significance by Mann-Whitney

U test with correction for multiple comparisons; only significant *p*-values after correction shown. **(h, i)** ILC3 quantification in the FFPE lung sections from human, non-human primates (active and latent) was carried out by staining with CD3, B220 and Rorγt and the number of Rorγt^{+}CD3^{-} (ILC3) and Rorγt^{+}CD3^{+} (Th17) cells were counted and shown. Data shown as mean ± SD. Significance by Student's *t*-test **(i)**

Figure 3. ILCs demonstrate a structured response to pulmonary TB at the transcriptomic level. (a) ILC2s and ILC3s were sorted from lung tissue and differential gene expression between TB infected (n=5) and uninfected control tissue (n=2) were determined by RNA sequencing. (**b**) Expression of key chemokines and chemoattractant proteins significantly upregulated in pulmonary ILCs from TB participants (Pos, n=5) when compared to uninfected control lungs is shown (Neg, n=2). *p*-values corrected using Benjamini-Hochberg with a significance cut-off of FDR < 0.01. **(c)** Upstream drivers of differentially expressed genes in ILC2s and ILC3s were predicted using Ingenuity Pathway Analysis (IPA). *p*-values calculated by hypergeometric test between genes in our data and known interactions in the literature for each driver. (**d**) VIP and (**e**) OSM protein expression was confirmed *in situ* in TB-infected human lung tissues using multiplexed fluorescent immunohistology. (**f**) The network of upstream drivers enriched in the differentially expressed genes in sorted ILC3s between TB infected and uninfected samples is shown. Inset: GO Network generated over the genes identified as downstream of *OSM* by IPA (n=64, see **Methods**). Each node represents a specific GO/KEGG/Reactome term (**Extended Data Table. 4**). Broad categories of pathways are annotated. Line width/darkness corresponds to number of shared genes between nodes. Node size: ** p<0.01, *** p<0.001. **(g)** Select predicted downstream pathways enriched in the differentially expressed genes in ILC3s between TB infected and uninfected samples are shown.

Figure 4. ILCs mediate iBALT formation and contribute to early protection from *Mtb*. *Rag1*$^{-/-}$, *Rag2γc*$^{-/-}$ and wild type mice were aerosol infected with ~100 CFU *Mtb.* ILCs (CD45^{+}CD127^{+}Lin^{-}NK1.1^{-}) were isolated from *Mtb* infected wild type mice and ~5X10^3 cells

were intratracheally transferred into *Rag2γc*$^{-/-}$ mice 1 day before infection. **(a)** Lung bacterial burden at 14 dpi was determined by plating (n=5/group). (**b**) Number of ILC1s, ILC2s, total ILC3s and NKp46^{+} ILC3s and (**c**) AMs were measured by flow cytometry. (**d**) ILC3 quantification in histological lung sections was carried out by staining with CD3, B220 and Rorγt and the number of Rorγt^{+}CD3^{-} ILC3s were counted and shown. **(e)** *Ahr*$^{f/f}$, *Ahr*$^{f/f}$*Rorγt*^{Cre} mice were aerosol infected with ~100 CFU *Mtb and* lung bacterial burden at 14 and 30 dpi was determined by plating (n=7-10/group). (**f**) Number of ILC1s, ILC2s, total ILC3s, NKp46^{+} ILC3s and AMs were enumerated by flow cytometry. **(g)** Lung cells from B6 mice were infected in vitro with MOI 0.1 *Mtb* and IL-23 (n=3/UI, n=4/*Mtb*) protein levels were measured in supernatants on 5 dpi and compared to uninfected (UI) cells. **(h, left).** Lung cells from B6 mice were infected in vitro with MOI 0.1 *Mtb as before and* stimulated with recombinant (r) IL-23, rIL-1β and the protein levels of IL-22 and IL-17 were measured in supernatants and compared with levels in uninfected (UI) cells and **(h, right)** the numbers of IL-17 and IL-22 producing ILCs were measured by flow cytometry. **(i)** B6 and *IL-17/22*$^{-/-}$ were aerosol infected with ~100 CFU *Mtb* and lung bacterial CFU were measured by plating (n=12/group). **(j)** Number of ILC1, ILC2, ILC3, CXCR5^{+} ILC3, and CXCR5^{+}NKp46^{+} ILC3 were measured by flow cytometry (n=5/B6, n=8/*IL-17/22*$^{-/-}$). (**k**) FFPE lung sections were subjected to in situ hybridization (ISH) with the mouse-CXCL13 probe and the ratio of CXCL13 mRNA^{+} area occupied per lung was quantified. **(l)** B6 mice received IL-23 blocking antibody (i.p.) -1 day prior to infection with ~100 CFU *Mtb* and the lung bacterial burden and (**m)** number of AMs, ILC2s and ILC3s were quanified at 14 dpi using plating and flow cytometry respectively (n=5/isotype, n=5-6/anti-IL-23). Iso = Isotype. **(n)** FFPE lung sections from 30 dpi *Mtb* infected mice were stained with antibodies to B220 and CD3, and the average size of B-cell follicles were quantified in *Ahr*$^{f/f}$, *Ahr*$^{f/f}$*Rorγt*^{Cre}, B6, *IL-17/22*$^{-/-}$, isotype-treated B6 and anti IL-23-treated B6 *Mtb*-infected mice. All data shown as mean ± SD. Significance by either one way ANOVA (**a-d**) or Student's *t*-test (**e-n**).

Extended Data Figure 1. Hierarchical gating strategy used to identify lymphocyte populations in human blood and lung samples. Single cells from blood or lung samples from human participants were processed for flow cytoometry, and all doublets were excluded. Cells were gated as lymphocytes, live, $CD45^+$ and $CD3^+$ T cells or $CD3^-$ cells. $CD3^-$ cells were gated on CD56 and CD94. $CD94^+$ cells are NK cells and were further sub-gated as $CD16^-CD56^{hi}$ NK cells or $CD16^+CD56^{dim}$ NK cells. ILCs in the $CD94^-$ fraction were $CD127^+$ and negative for all lineage markers CD4, CD11c, CD14, CD19, CD34, FcER1, BDCA2, TCR$\alpha\beta$ and TCR$\gamma\delta$. Total ILCs were $CD127^+CD161^+$, ILC2 were $Lin^-CD127^+CRTH2^+$ cells. ILC1 were $Lin^-CD127^+CRTH2^-CD56^-CD117^-$ cells. ILC3 were $Lin^-CD127^+CRTH2^-CD117^+$ cells with variable CD56 expression.

Extended Data Figure 2. ILC depletions seen in TB participants are not affected by TB drug resistance or concurrent HIV infection. (a) The frequencies of the two main circulating NK populations, $CD16^+CD56^{dim}$ and $CD16^-CD56^{hi}$ were measured in human participants with TB and healthy controls by flow cytometry. NK cell frequencies in paired samples taken from the same TB participant before and after 6 months of standard and successful TB therapy were also determined by flow cytometry. **(b)**. Percentages of blood ILC1, ILC2, ILC3, $CD56^{dim}$ NK cells, and $CD56^{hi}$ NK cells in TB^-HIV^- control subjects, TB participants without (TB^+HIV^-) and with HIV co-infection (TB^+HIV^+), and multi-drug resistant TB participants without ($MDRTB^+HIV^-$) and with HIV co-infection ($MDRTB^+HIV^+$) were measured. Significance calculated by a Dunn's multiple comparison test. Where *p*-value not shown, **p*<0.05, ***p*<0.01. (**c**) Capase-3 expression in circulating lymphocytes from peripheral blood of TB participants and controls was done by flow cytometry. Significance calculated using a Mann-Whitney U test.

Extended Data Figure 3. Hierarchical mouse lung ILC flow gating strategy. (a-c) B6 mice were aerosol infected with ~100 CFU *Mtb* and lungs were harvested at different dpi. for flow cytometric analysis. Flow gating strategy for **(a)** ILC1 ($CD45^+CD127+Lin^-NKp46^+NK1.1^+$), **(b)** ILC2 ($CD45^+CD127^+Lin^-NK1.1^-ScaI^+$), and ILC3 ($CD45^+CD127^+Lin^-NK1.1^-Ror\gamma t^+$) and NKp46-

712 expressing ($CD45^+CD127^+Lin^-NK1.1^-Ror\gamma t^+NKp46^+$) ILC3 cells are shown. (**c**) *Rorγt-eGFP*
713 mice were aerosol infected with ~100 CFU *Mtb* and lungs were harvested at 14 dpi. ILC3
714 ($CD45^+CD127^+Lin^-NK1.1^-GFP^{+)}$ populations were quantified using flow cytometry.

715 **Extended Data Figure 4. Pulmonary ILCs are tissue resident and express markers of**
716 **migration. (a)** CD69, CD103, CD62L and NKp44 expression on the circulating ILCs in human
717 peripheral blood and lung tissue were measured by flow cytometry. Significance by unpaired
718 Mann-Whitney U test. Percentage of total human ILCs expressing these markers in paired
719 samples of TB participants shown. Significance calculated using a one-way Wilcoxon-
720 matched paired test. **(b,c)** NKp44, CD56 expression were measured in TB-infected lung
721 tissues in comparison to control samples. Significance by unpaired Mann-Whitney U test (b)
722 and a Kruskal-Wallis test with adjustments for multiple comparisons (c). (**d**) Percentages of
723 ILC1, ILC2, ILC3, $CD56^{dim}$ NK cells, and $CD56^{hi}$ NK cells in human lung tissue were measured
724 by flow cytometry TB^-HIV^- control subjects, TB participants without (TB^+HIV^-) and with HIV co-
725 infection (TB^+HIV^+). **(e)** CXCL13 protein levels were measured in the plasma from TB
726 participants without (TB^+HIV^-) and with HIV co-infection (TB^+HIV^+). Significance calculated by
727 Mann-Whitney U test (no significance after Bonferonni correction). **(f)** Frequencies of $CD103^+$
728 ILCs were measured by flow cytometry in the blood from TB^-HIV^- control subjects, TB
729 participants without (TB^+HIV^-) and with HIV co-infection (TB^+HIV^+). Significance by Mann-
730 Whitney U test with Bonrefonni corrections (only significant values after correction shown). **(g)**
731 Representative FACS plots showing two distinct subpopulations of CD103 and CXCR5-
732 expressing ILCs measured in lung tissues from three TB+ve subjects, where most CXCR5-
733 expressing cells are $CD117^+$ ILC3s, and $CD103^+$ lung ILCs are a combination of $CD117^+$
734 ILC3s, $CRTH2^+$ ILCs and $CD117^-CRTH2^-$ cells. Green = $CD117^+$; Red = $CRTH2^+$. (**h**) B6 mice
735 were aerosol infected with ~100 CFU *Mtb* and lungs were harvested at 14 dpi. Lung ILCs were
736 sorted from single cell suspensions (ILCs: $CD45^+$ $CD127^+Lin^-NK1.1^-$). The ability of sorted
737 ILCs to migrate towards media alone or mouse CXCL13 gradient was quantitated in transwell
738 migration assay. N=3-5 biological replicates. Significance by One way ANOVA, *p<0.05,

739 **p<0.01. (**i**) Human ILC3s sorted from lungs migrated in response to recombinant human
740 CXCL13 in transwell migration assays. Significance by one tailed t-test.

741 **Extended Data Figure 5.** IHC staining for nuclear Rorγt, CD3, and PAX5 on paraffin-
742 embedded formalin fixed lung tissues from **(a, left)** PTB or influenza-infected human
743 participants, **(a, right)** latent TB infected (LTBI) and actively infected (PTB) non-human
744 primates (NHPs). **(b)** Representative fluorescent immunohistology scans of TB-infected
745 human and non human primate lung tissues, with CD20 (FITC), CD3 (PE-Texas Red) and
746 CD127(PE-Cy5). $CD3^-CD127^+$ ILCs are present adjacent to follicles (upper panels) and
747 granuloma-like structures (lower panels). (**c**) Total numbers of ILCs/mm^2 of tissue are
748 increased in structures of TB histopathlogy (combined lesional tissue) in comparision to
749 remainder of unaffected tissue (Non-Lesional). But percentages of ILCs per total cell number
750 ($DAPI^+$ cells) are not different between regions of interest (Lesional tissue) and unaffected
751 tissue (Non-Lesional).

752 **Extended Data Figure 6. Sort purity of human ILC3 and $CD4^+$ T cells.** ILC3s and $CD4^+$ T
753 cells were sorted from human PBMCs and reflowed back into FACSARIA fusion to confirm
754 purity. Purity of ILC3s confirmed as 100% and $CD4^+$ T cells sort was 97% pure.

755 **Extended Data Figure 7. Sorting purity of mouse ILCs. (a)** B6 mice were aerosol infected
756 with ~100 CFU *Mtb* and lungs were harvested at 5 dpi. Lung CD45 population was encriched
757 by using CD45 Microbeads. CD45 enriched cells were stained and lung ILCs
758 ($CD45^+CD127^+Lin^-NK1.1^-$) were purified by using FACSJazz. Sort purity is shown here. (**b**)
759 mRNA expression of *CCR6*, *Rorc* and *Ahr* relative to GAPDH on the purified ILCs was
760 quantitated by RT-PCR.

761 **Extended Data Figure 8. ILC1 and ILC2 are dispensable for early protection against**
762 **tuberculosis. (a, c)** B6, *IFNγ$^{-/-}$, IL-13$^{-/-}$ and Rorγ$^{-/-}$* mice were aerosol infected with ~100 CFU
763 *Mtb* and at 14 days post infection bacterial burden was measured in the lungs by plating. (**b,**

d) Numbers of lung ILC1s, ILC2s and ILC3s were quantified by using flow cytometry. Significance by One way ANOVA (**a, b**) or student's t-test (**c,d**).

Extended Data Figure 9. NKP46^{+} ILC3s contribute to early protection from *Mtb*. (a) *Cbfb$^{f/f}$NKp46^{Cre}* and *Cbfb$^{f/f}$* mice were aerosol infected with ~100 CFU *Mtb* and at 14 and 30 dpi (**a**) bacterial burden was determined in the lungs by plating. (**b**) Numbers of lung ILC1s, ILC2s, ILC3s and AMs were determined by using flow cytometry. (**c**) FFPE lung sections from 30 dpi *Mtb* infected mice were stained with antibodies to B220 and CD3, and the average size of B-cell follicles were quantified. (**d**) Uninfected *Cbfb$^{f/f}$NKp46^{Cre}* and *Cbfb$^{f/f}$* mice were harvested, and lung and lymph nodes were analyzed for the different myeloid (AMs, mDCs, neutrophils, monocytes and recruited macrophages) and (**e**) T cell ($CD3^{+}CD4^{+}$, $CD3^{+}CD8^{+}$, $CD3^{+}TCR\alpha^{+}$, $CD3^{+}\gamma\delta^{+}$) populations by flow cytometry. Significance by Student's t-test.

Extended Data Figure 10. Natural killer cells are dispensable during *Mtb* infection. B6 mice were aerosol infected with ~100 CFU *Mtb* and treated with isotype (n=5) or anti-NK1.1 (n=5, PK126, 100 μg) every 3 days. **(a)** Lung natural killer (NK) cells were determined following treatment with isotype or anti-NK1.1 at 30 dpi. by flow cytometry. **(b)** Lung bacterial burden was assessed at 30 dpi. All data shown as mean ± SEM. Significance calculated by Student's *t*-test **(a-b)**.

Extended Data Figure 11. No baseline defects observed in lung populations in Rorγt^{cre}/Ahr$^{f/f}$. (a-g) Uninfected *Ahr$^{f/f}$* and *Rorγt^{cre}Ahr$^{f/f}$* mice were harvested, and lung and lymph nodes were analyzed for the different myeloid (AMs, mDCs, neutrophils, monocytes and recruited macrophages) and (**e**) T cell ($CD3^{+}CD4^{+}$, $CD3^{+}CD8^{+}$, $CD3^{+}TCR\alpha^{+}$, $CD3^{+}\gamma\delta^{+}$) populations by flow cytometry. All data shown as mean ± SD. Significance by Student's t- test.

Extended Data Figure 12. CXCR5 deficiency increases susceptibility to *Mtb* infection. (**a**) B6 and *CXCR5$^{-/-}$* mice were aerosol infected with ~100 CFU *Mtb* and at 30 dpi bacterial burden was determined in the lungs by plating. (**b**) ILC3 quantification in FFPE lung sections was carried out by staining with CD3, B220 and Rorγt and the number of Rorγt^{+}CD3^{-} ILC3

were counted and shown. (**c**) FFPE lung sections from 30 dpi *Mtb* infected mice were stained with antibodies to B220 and CD3, and the average size of B-cell follicles were quantified. Significance by Student's *t*-test.

Supplementary Table 1. Differentially expressed genes of ILC2s sorted from TB-infected and control lungs. ILC2 were sorted from lung tissue and differential gene expression between TB infected (n=5) and uninfected control tissue (n=2) were determined by RNA sequencing. *p*-values corrected using Benjamini-Hochberg with a significance cut-off of FDR < 0.01.

Supplementary Table 2. Differentially expressed genes of ILC3s sorted from TB-infected and control lungs. ILC3s were sorted from lung tissue and differential gene expression between TB infected (n=5) and uninfected control tissue (n=2) were determined by RNA sequencing. *p*-values corrected using Benjamini-Hochberg with a significance cut-off of FDR < 0.01.

Supplementary Table 3. Predicted upstream drivers of DE response in ILC2s. Upstream drivers of differentially expressed genes in ILC2s were predicted using Ingenuity Pathway Analysis (IPA). *p*-values calculated by hypergeometric test between genes in our data and known interactions in the literature for each driver.

Supplementary Table 4. Predicted upstream drivers of DE response in ILC3s. Upstream drivers of differentially expressed genes in ILC3s were predicted using Ingenuity Pathway Analysis (IPA). *p*-values calculated by hypergeometric test between genes in our data and known interactions in the literature for each driver.

Supplementary Table 5. Downstream driver network for genes known to interact with OSM. Network created using the Mechanistic Networks generated by IPA, using a *p*-value< 0.01 for overlap significance.

Supplementary Table 6. Select predicted downstream pathways enriched in the differentially expressed genes in ILC3s between TB infected and uninfected samples. Generated in IPA.

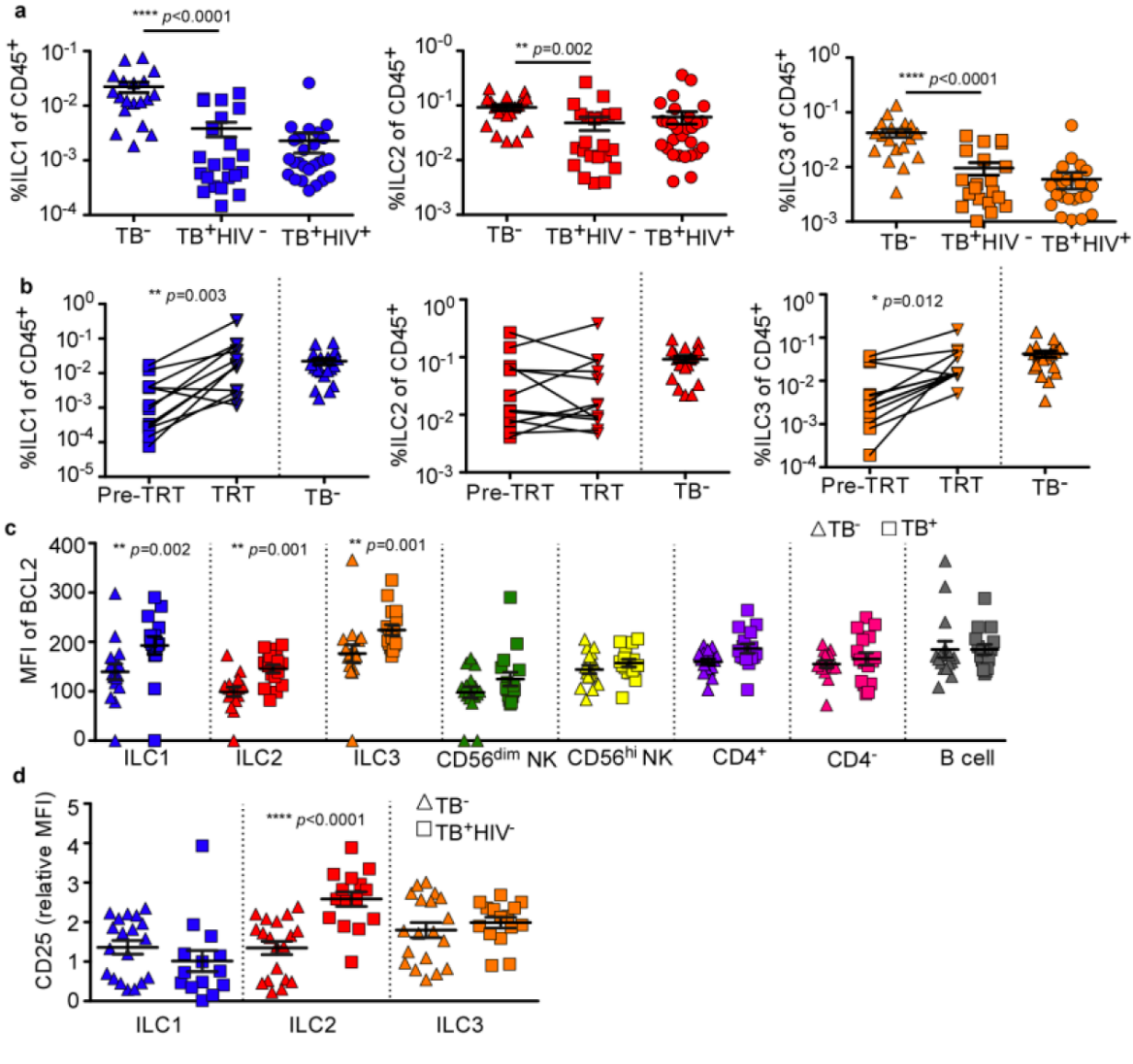
a
**** p<0.0001
%ILC1 of CD45+
TB-
TB+HIV -
TB+HIV+
** p=0.002
%ILC2 of CD45+
**** p<0.0001
%ILC3 of CD45+
b
** p=0.003
%ILC1 of CD45+
Pre-TRT
TRT
TB-
%ILC2 of CD45+
* p=0.012
%ILC3 of CD45+
c
△TB- □TB+
** p=0.002
** p=0.001
** p=0.001
MFI of BCL2
ILC1
ILC2
ILC3
CD56dim NK
CD56hi NK
CD4+
CD4-
B cell
d
△TB-
□TB+HIV-
**** p<0.0001
CD25 (relative MFI)
ILC1
ILC2
ILC3

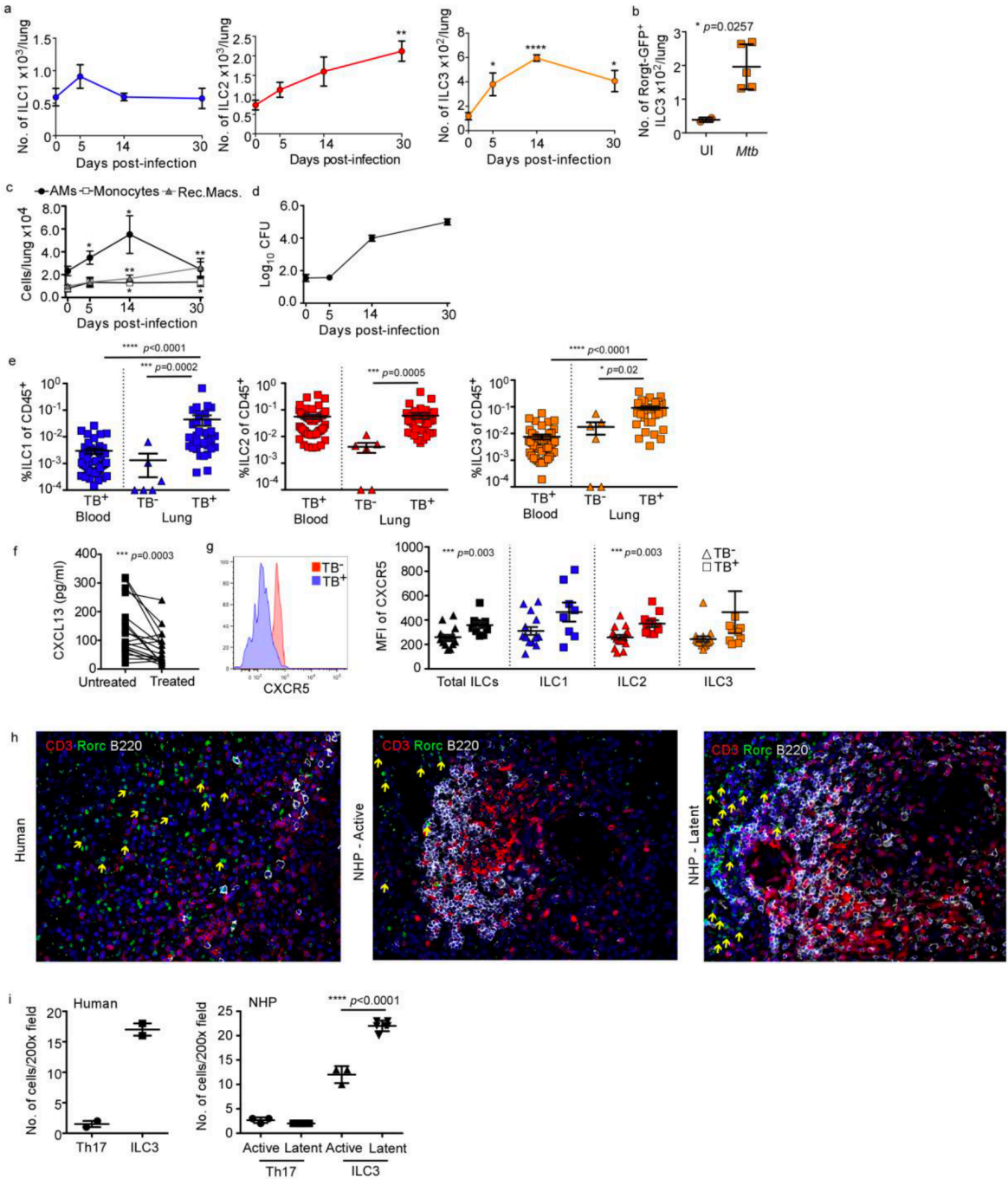
a
No. of ILC1 x10^3/lung
No. of ILC2 x10^3/lung
No. of ILC3 x10^2/lung
Days post-infection
b
* p=0.0257
No. of Rorgt-GFP+ ILC3 x10^-2/lung
UI
Mtb
c
AMs Monocytes Rec.Macs.
Cells/lung x10^4
d
Log10 CFU
e
**** p<0.0001
*** p=0.0002
*** p=0.0005
* p=0.02
%ILC1 of CD45+
%ILC2 of CD45+
%ILC3 of CD45+
TB+ Blood
TB- Lung
TB+ Lung
f
*** p=0.0003
CXCL13 (pg/ml)
Untreated
Treated
g
TB-
TB+
CXCR5
MFI of CXCR5
Total ILCs
ILC1
ILC2
ILC3
h
CD3 Rorc B220
Human
NHP - Active
NHP - Latent
i
Human
No. of cells/200x field
Th17
ILC3
NHP
**** p<0.0001
Active
Latent

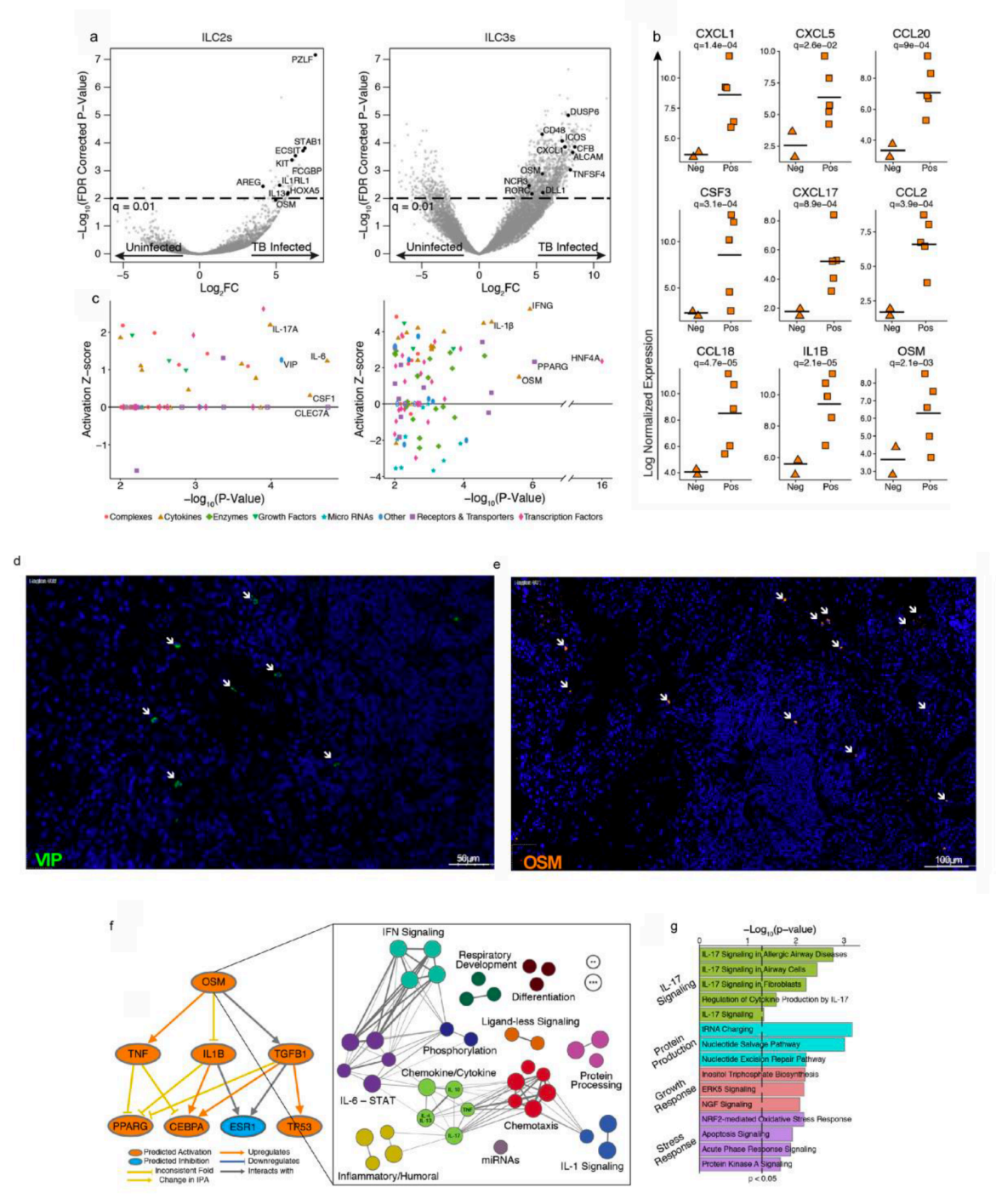
a
ILC2s
ILC3s
−Log10(FDR Corrected P−Value)
Log2FC
q = 0.01
Uninfected
TB Infected
PZLF
STAB1
ECSIT
KIT
FCGBP
AREG
IL1RL1
IL13
HOXA5
OSM
DUSP6
CD48
ICOS
CXCL1
CFB
ALCAM
TNFSF4
NCR3
RORC
DLL1
b
Log Normalized Expression
CXCL1
q=1.4e−04
CXCL5
q=2.6e−02
CCL20
q=9e−04
CSF3
q=3.1e−04
CXCL17
q=8.9e−04
CCL2
q=3.9e−04
CCL18
q=4.7e−05
IL1B
q=2.1e−05
OSM
q=2.1e−03
Neg
Pos
c
Activation Z−score
−log10(P-Value)
IL-17A
IL-6
VIP
CSF1
CLEC7A
IFNG
IL-1β
HNF4A
PPARG
OSM
Complexes
Cytokines
Enzymes
Growth Factors
Micro RNAs
Other
Receptors & Transporters
Transcription Factors
d
VIP
50 µm
e
OSM
100 µm
f
OSM
TNF
IL1B
TGFB1
PPARG
CEBPA
ESR1
TP53
Predicted Activation
Predicted Inhibition
Inconsistent Fold
Change in IPA
Upregulates
Downregulates
Interacts with
IFN Signaling
Respiratory Development
Differentiation
Ligand-less Signaling
Phosphorylation
Chemokine/Cytokine
IL-6 – STAT
Protein Processing
Chemotaxis
miRNAs
IL-1 Signaling
Inflammatory/Humoral
g
−Log10(p−value)
IL-17 Signaling
Protein Production
Growth Response
Stress Response
IL-17 Signaling in Allergic Airway Diseases
IL-17 Signaling in Airway Cells
IL-17 Signaling in Fibroblasts
Regulation of Cytokine Production by IL-17
IL-17 Signaling
tRNA Charging
Nucleotide Salvage Pathway
Nucleotide Excision Repair Pathway
Inositol Trisphosphate Biosynthesis
ERK5 Signaling
NGF Signaling
NRF2-mediated Oxidative Stress Response
Apoptosis Signaling
Acute Phase Response Signaling
Protein Kinase A Signaling
p < 0.05

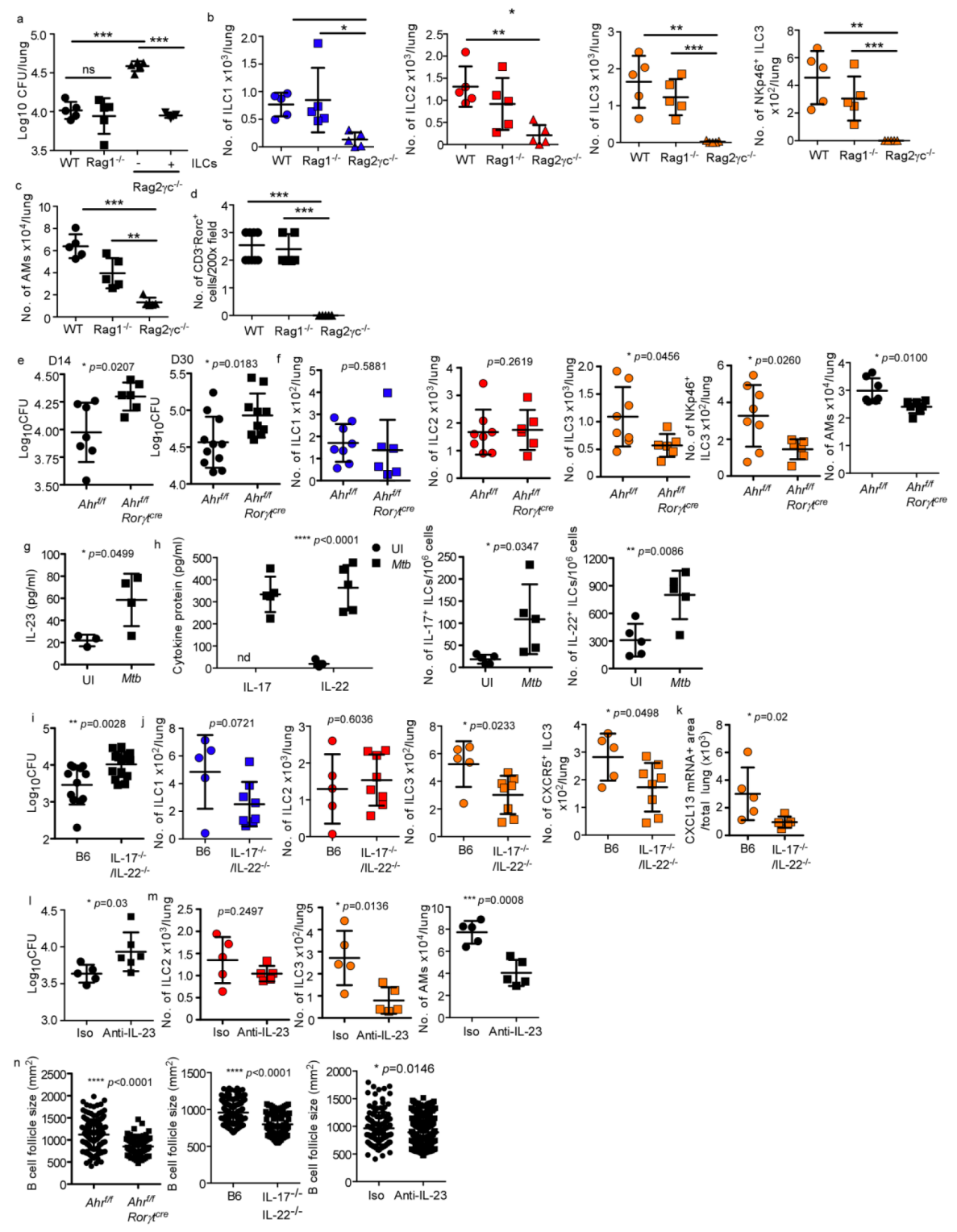
a
Log10 CFU/lung
***
***
ns
WT Rag1-/- - + ILCs
Rag2γc-/-
b
No. of ILC1 x10³/lung
No. of ILC2 x10³/lung
No. of ILC3 x10³/lung
No. of NKp46+ ILC3 x10²/lung
WT Rag1-/- Rag2γc-/-
c
No. of AMs x10⁴/lung
d
No. of CD3-Rorc+ cells/200x field
e
D14
D30
Log10CFU
* p=0.0207
* p=0.0183
Ahrf/f
Ahrf/f Rorγtcre
f
No. of ILC1 x10²/lung
p=0.5881
No. of ILC2 x10³/lung
p=0.2619
No. of ILC3 x10³/lung
* p=0.0456
No. of NKp46+ ILC3 x10²/lung
* p=0.0260
No. of AMs x10⁴/lung
* p=0.0100
g
IL-23 (pg/ml)
* p=0.0499
UI
Mtb
h
Cytokine protein (pg/ml)
**** p<0.0001
UI
Mtb
nd
IL-17
IL-22
No. of IL-17+ ILCs/10⁶ cells
* p=0.0347
No. of IL-22+ ILCs/10⁶ cells
** p=0.0086
i
Log10CFU
** p=0.0028
B6
IL-17-/- /IL-22-/-
j
No. of ILC1 x10²/lung
p=0.0721
No. of ILC2 x10³/lung
p=0.6036
No. of ILC3 x10²/lung
* p=0.0233
No. of CXCR5+ ILC3 x10²/lung
* p=0.0498
k
CXCL13 mRNA+ area /total lung (x10³)
* p=0.02
l
Log10CFU
* p=0.03
Iso
Anti-IL-23
m
No. of ILC2 x10³/lung
p=0.2497
No. of ILC3 x10²/lung
* p=0.0136
No. of AMs x10⁴/lung
*** p=0.0008
n
B cell follicle size (mm²)
**** p<0.0001
**** p<0.0001
* p=0.0146

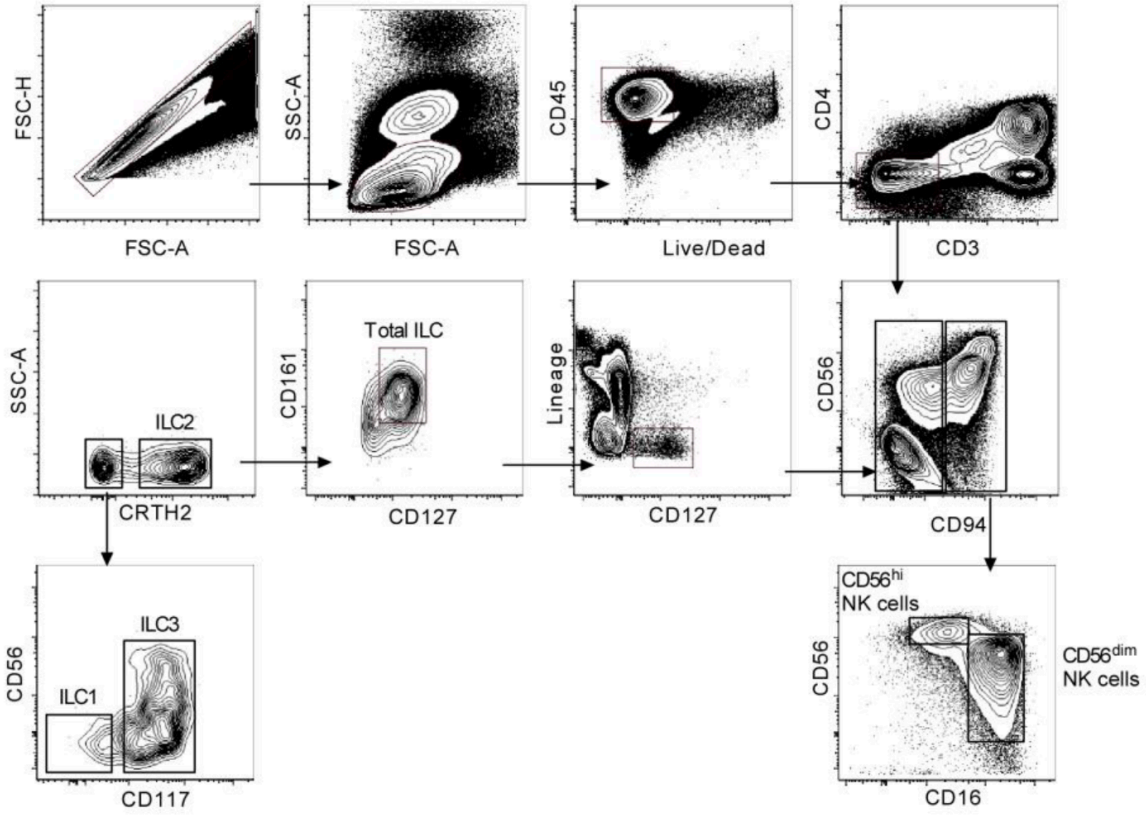
FSC-H
FSC-A
SSC-A
FSC-A
CD45
Live/Dead
CD4
CD3
SSC-A
ILC2
CRTH2
CD161
Total ILC
CD127
Lineage
CD127
CD56
CD94
CD56
ILC3
ILC1
CD117
CD56hi
NK cells
CD56dim
NK cells
CD56
CD16

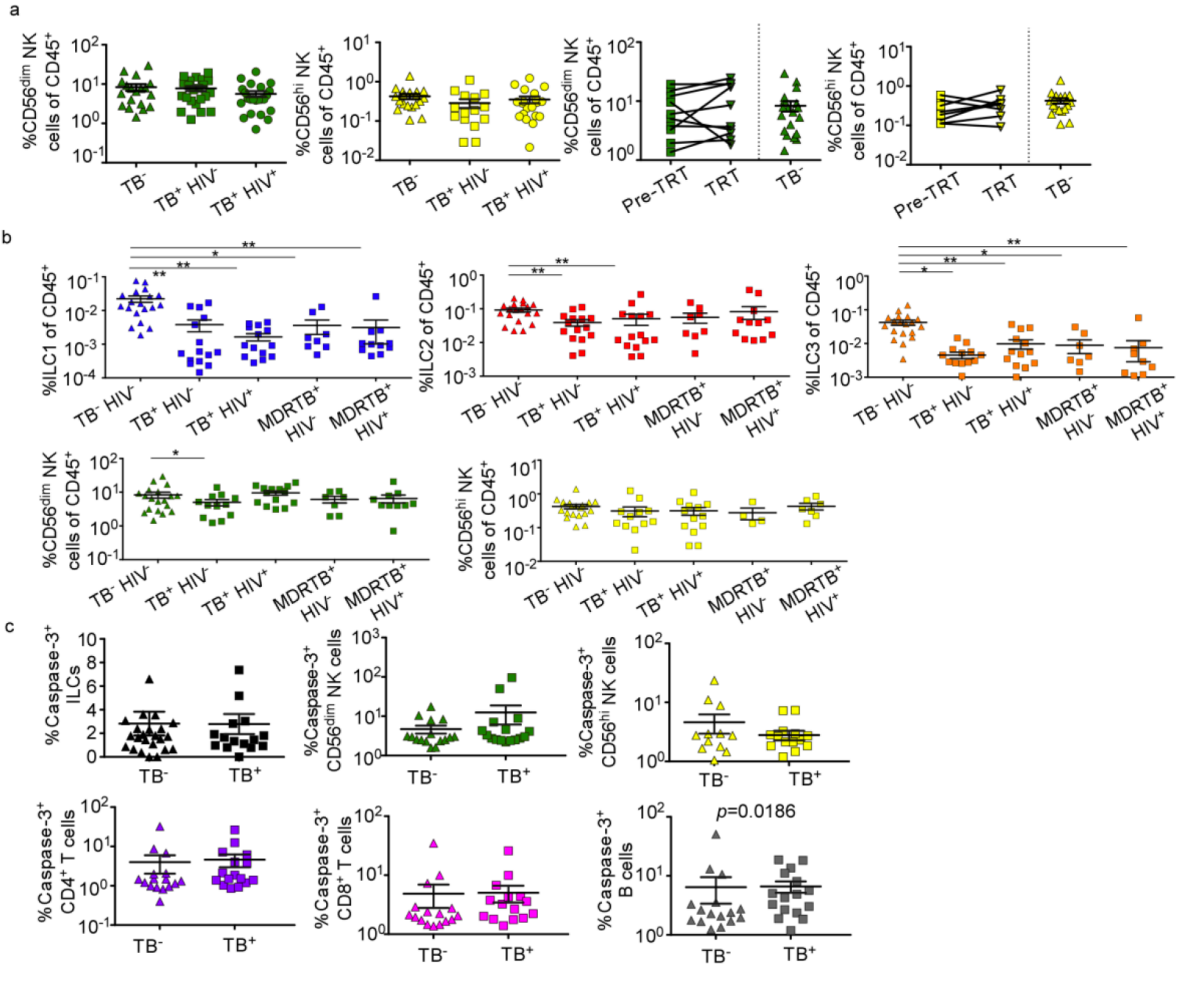
a
%CD56dim NK cells of CD45+
%CD56hi NK cells of CD45+
TB-
TB+ HIV-
TB+ HIV+
Pre-TRT
TRT
TB-
b
%ILC1 of CD45+
%ILC2 of CD45+
%ILC3 of CD45+
TB- HIV-
TB+ HIV-
TB+ HIV+
MDRTB+ HIV-
MDRTB+ HIV+
%CD56dim NK cells of CD45+
%CD56hi NK cells of CD45+
c
%Caspase-3+ ILCs
%Caspase-3+ CD56dim NK cells
%Caspase-3+ CD56hi NK cells
%Caspase-3+ CD4+ T cells
%Caspase-3+ CD8+ T cells
%Caspase-3+ B cells
p=0.0186
TB-
TB+

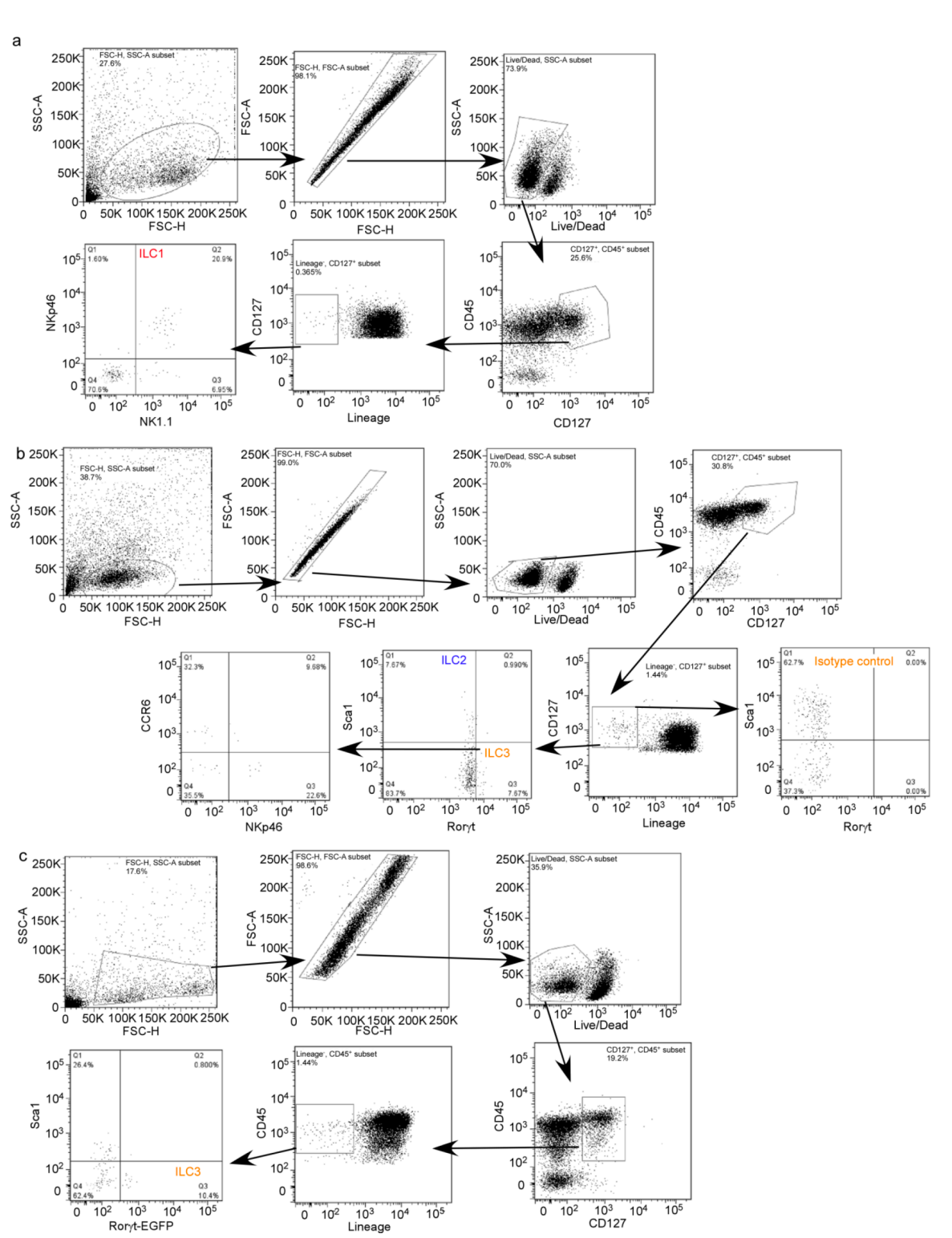
a
FSC-H, SSC-A subset
27.6%
FSC-H, FSC-A subset
98.1%
Live/Dead, SSC-A subset
73.9%
ILC1
Q1 1.60%
Q2 20.9%
Q4 70.6%
Q3 6.95%
Lineage⁻, CD127⁺ subset
0.365%
CD127⁺, CD45⁺ subset
25.6%
SSC-A
FSC-A
FSC-H
Live/Dead
NKp46
NK1.1
CD127
Lineage
CD45
b
FSC-H, SSC-A subset
38.7%
FSC-H, FSC-A subset
99.0%
Live/Dead, SSC-A subset
70.0%
CD127⁺, CD45⁺ subset
30.8%
ILC2
ILC3
Lineage⁻, CD127⁺ subset
1.44%
Isotype control
Q1 62.7%
Q2 0.00%
Q4 37.3%
Q3 0.00%
CCR6
Sca1
Rorγt
c
FSC-H, SSC-A subset
17.6%
FSC-H, FSC-A subset
98.6%
Live/Dead, SSC-A subset
35.9%
Lineage⁻, CD45⁺ subset
1.44%
CD127⁺, CD45⁺ subset
19.2%
Rorγt-EGFP

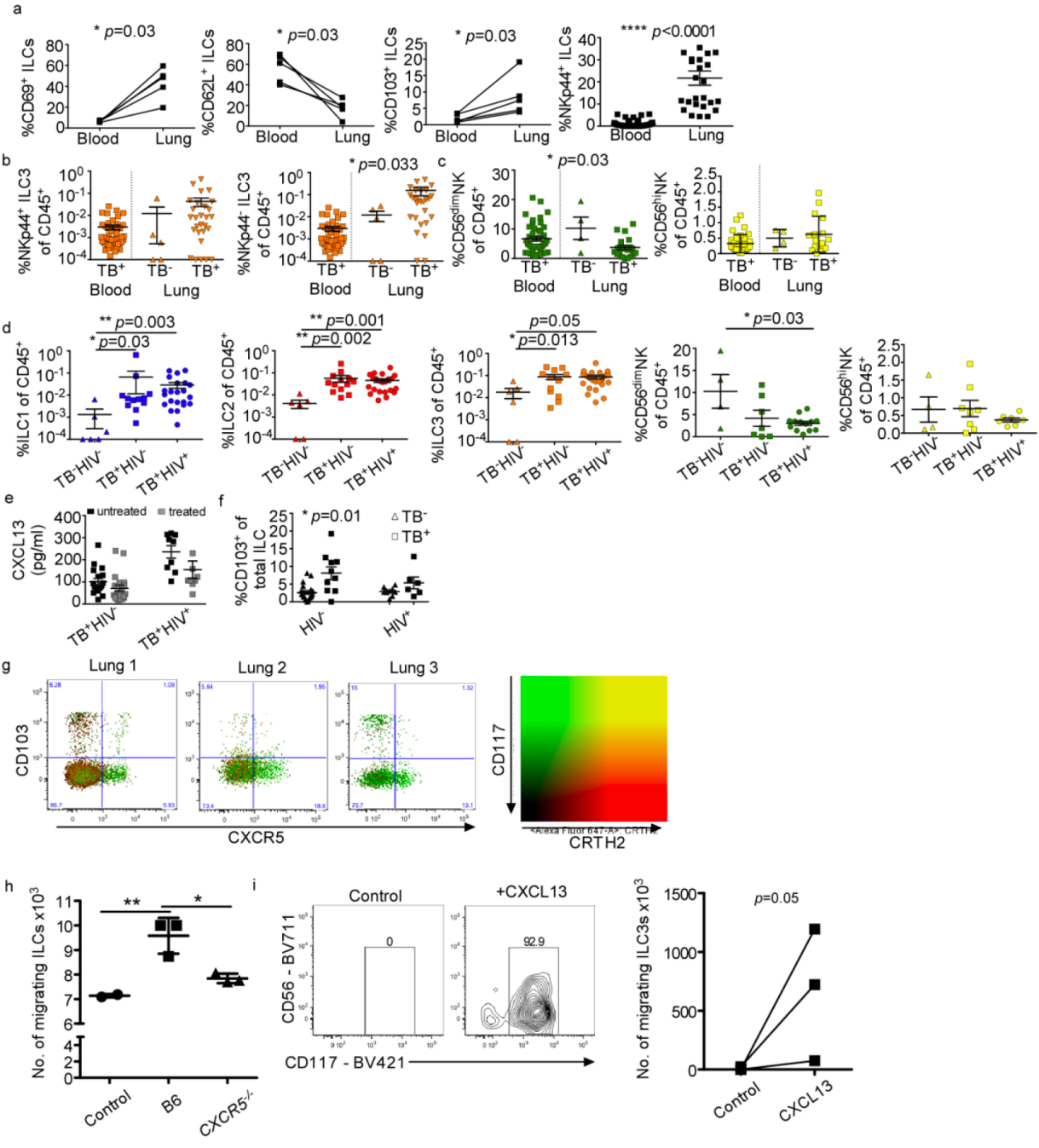
a
%CD69+ ILCs
* p=0.03
Blood
Lung
%CD62L+ ILCs
* p=0.03
%CD103+ ILCs
* p=0.03
%NKp44+ ILCs
**** p<0.0001
b
%NKp44+ ILC3 of CD45+
%NKp44- ILC3 of CD45+
* p=0.033
TB+
TB-
c
%CD56dimNK of CD45+
* p=0.03
%CD56hiNK of CD45+
d
%ILC1 of CD45+
** p=0.003
* p=0.03
%ILC2 of CD45+
** p=0.001
** p=0.002
%ILC3 of CD45+
p=0.05
* p=0.013
TB-HIV-
TB+HIV-
TB+HIV+
e
CXCL13 (pg/ml)
untreated
treated
f
%CD103+ of total ILC
* p=0.01
HIV-
HIV+
g
Lung 1
Lung 2
Lung 3
CD103
CXCR5
CD117
CRTH2
h
No. of migrating ILCs x10^3
**
*
Control
B6
CXCR5-/-
i
Control
+CXCL13
CD56 - BV711
CD117 - BV421
92.9
No. of migrating ILC3s x10^3
p=0.05
Control
CXCL13

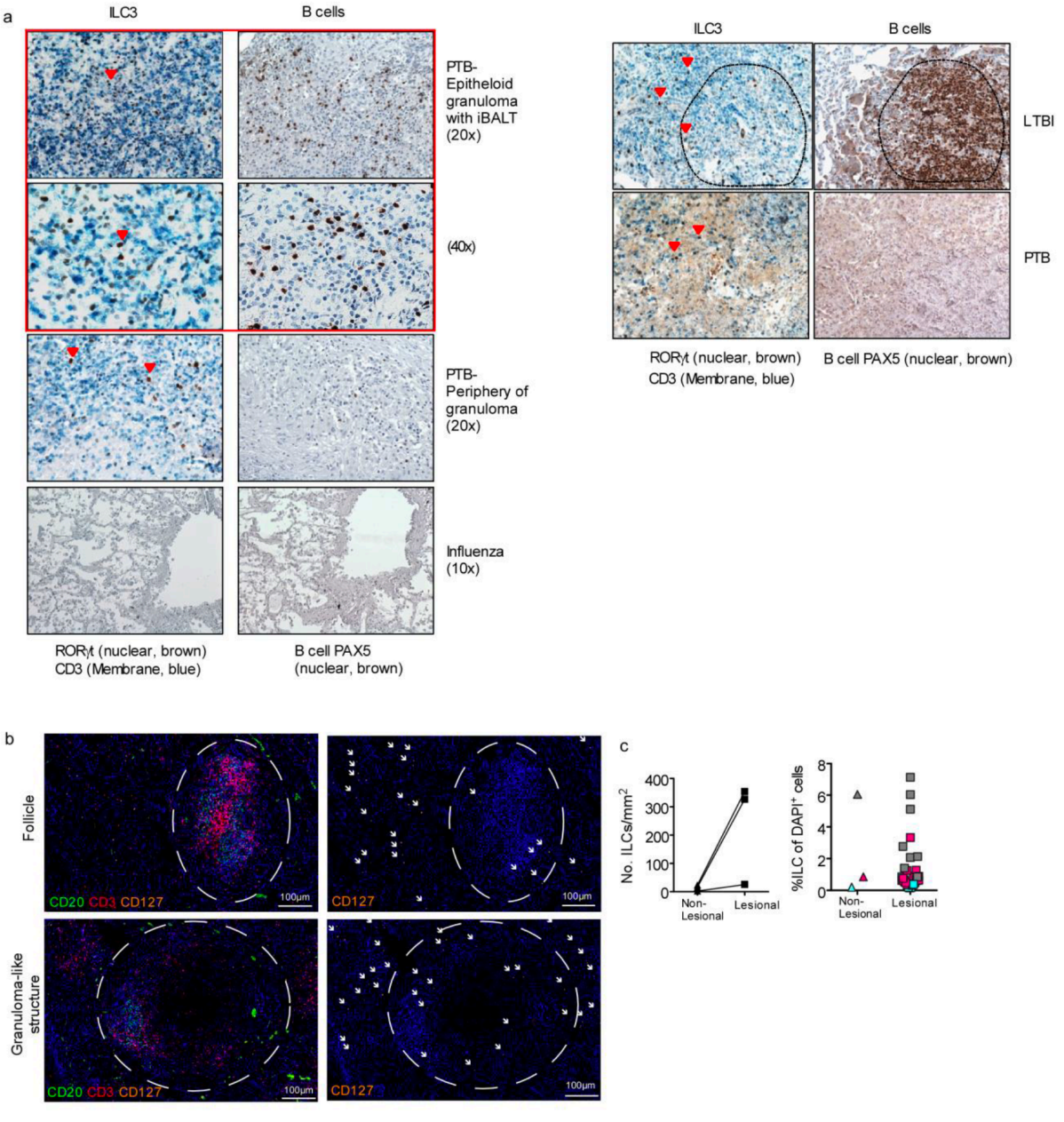
a
ILC3
B cells
PTB-Epitheloid granuloma with iBALT (20x)
(40x)
PTB-Periphery of granuloma (20x)
Influenza (10x)
RORγt (nuclear, brown)
CD3 (Membrane, blue)
B cell PAX5 (nuclear, brown)
ILC3
B cells
LTBI
PTB
RORγt (nuclear, brown)
CD3 (Membrane, blue)
B cell PAX5 (nuclear, brown)
b
Follicle
Granuloma-like structure
CD20 CD3 CD127
CD127
100μm
c
No. ILCs/mm2
400
300
200
100
0
Non-Lesional
Lesional
%ILC of DAPI+ cells
8
6
4
2
0
Non-Lesional
Lesional

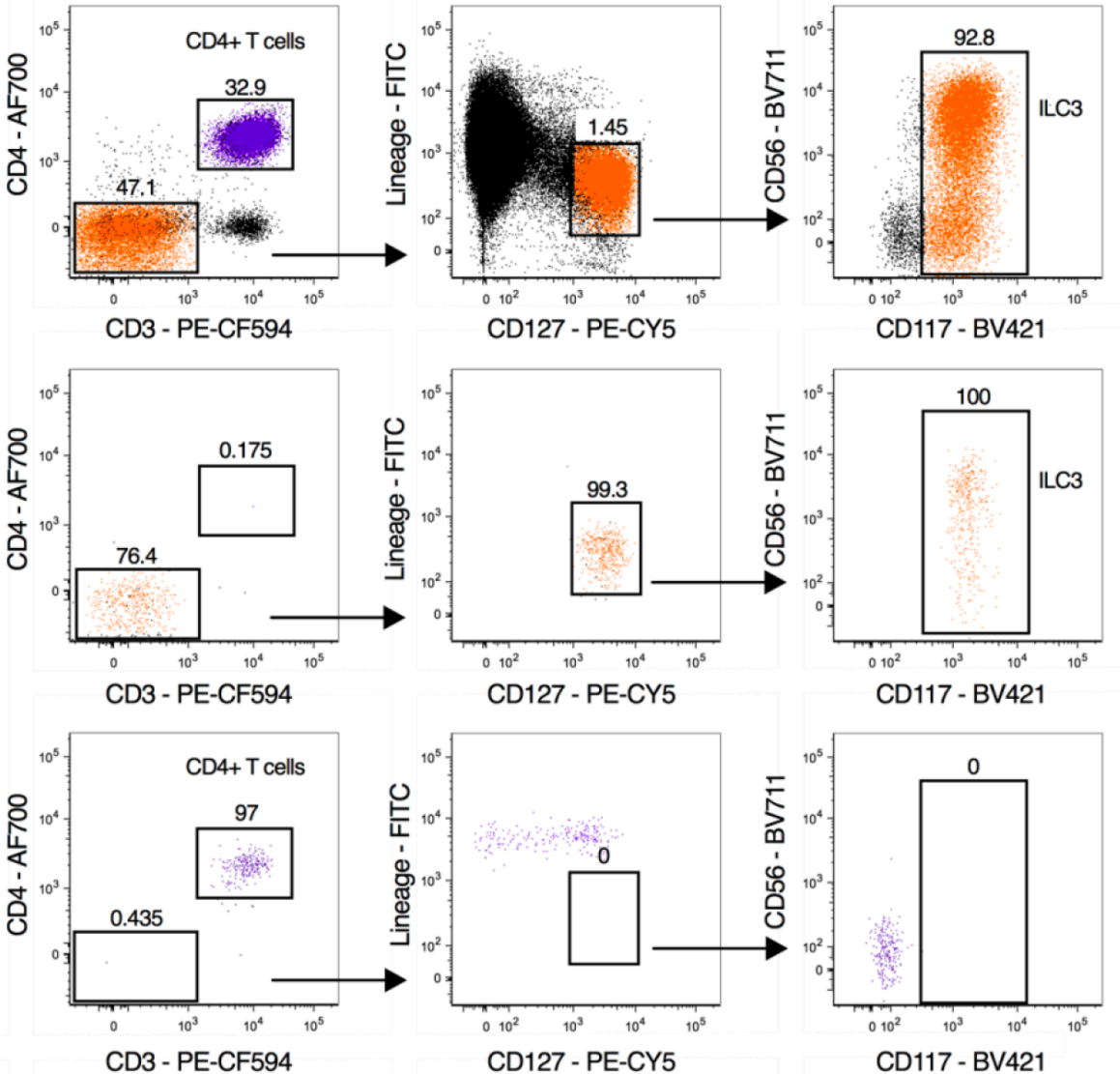
CD4+ T cells
32.9
47.1
CD4 - AF700
CD3 - PE-CF594
Lineage - FITC
1.45
CD127 - PE-CY5
CD56 - BV711
92.8
ILC3
CD117 - BV421
0.175
76.4
99.3
100
97
0.435
0

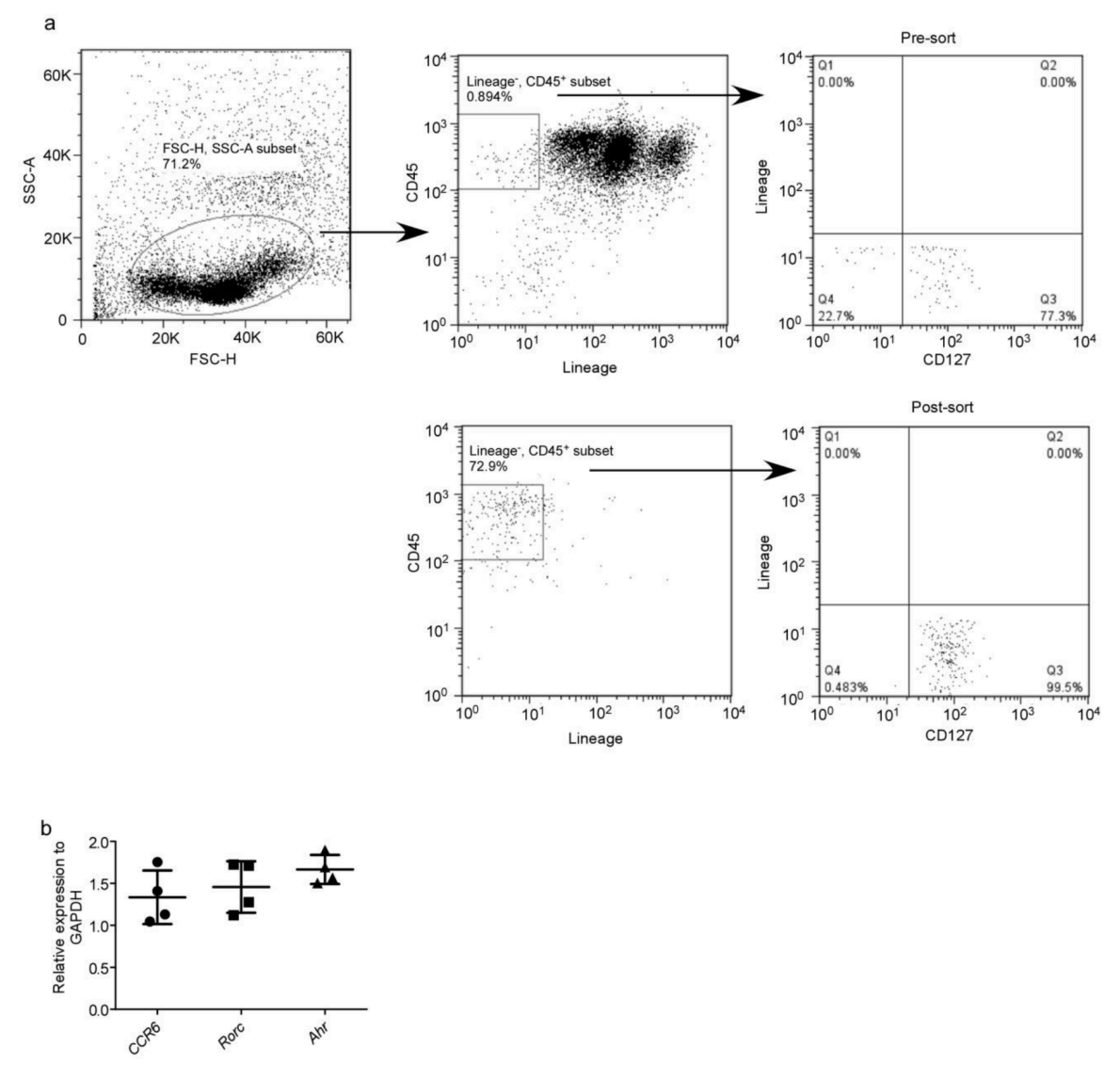
a
FSC-H, SSC-A subset
71.2%
SSC-A
FSC-H
Lineage⁻, CD45⁺ subset
0.894%
CD45
Lineage
Pre-sort
Q1
0.00%
Q2
0.00%
Q4
22.7%
Q3
77.3%
Lineage
CD127
Lineage⁻, CD45⁺ subset
72.9%
Post-sort
Q1
0.00%
Q2
0.00%
Q4
0.483%
Q3
99.5%
b
Relative expression to GAPDH
CCR6
Rorc
Ahr

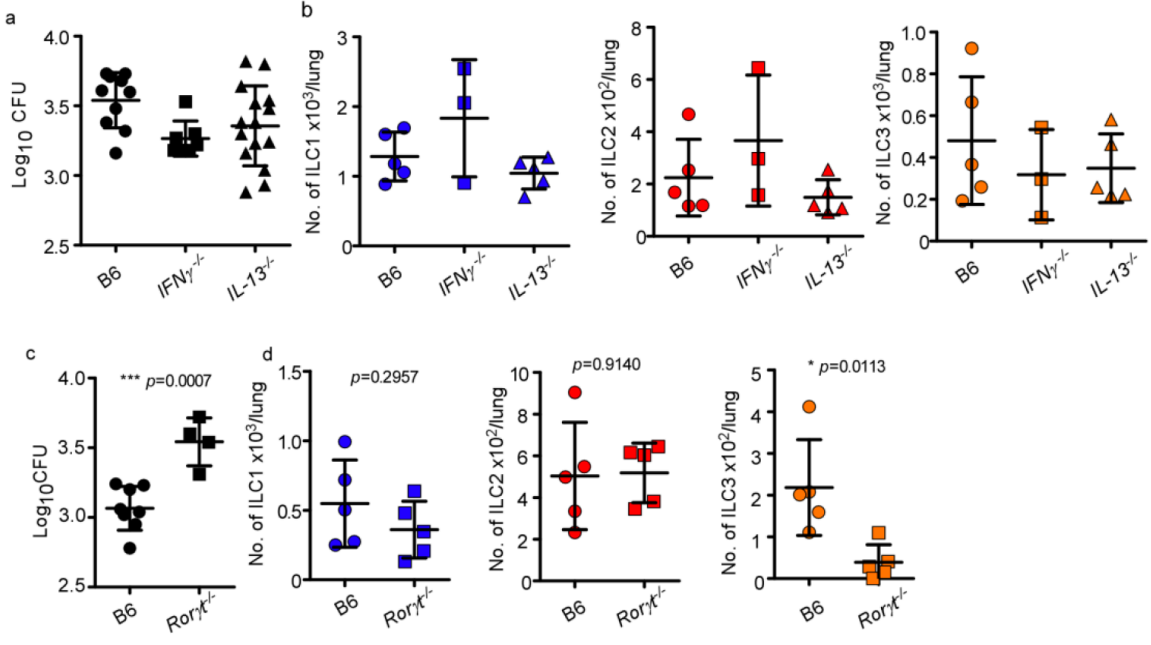
a
Log10 CFU
4.0
3.5
3.0
2.5
B6
IFNγ-/-
IL-13-/-
b
No. of ILC1 x10³/lung
No. of ILC2 x10²/lung
No. of ILC3 x10³/lung
c
Log10CFU
*** p=0.0007
d
p=0.2957
p=0.9140
* p=0.0113
Rorγt-/-

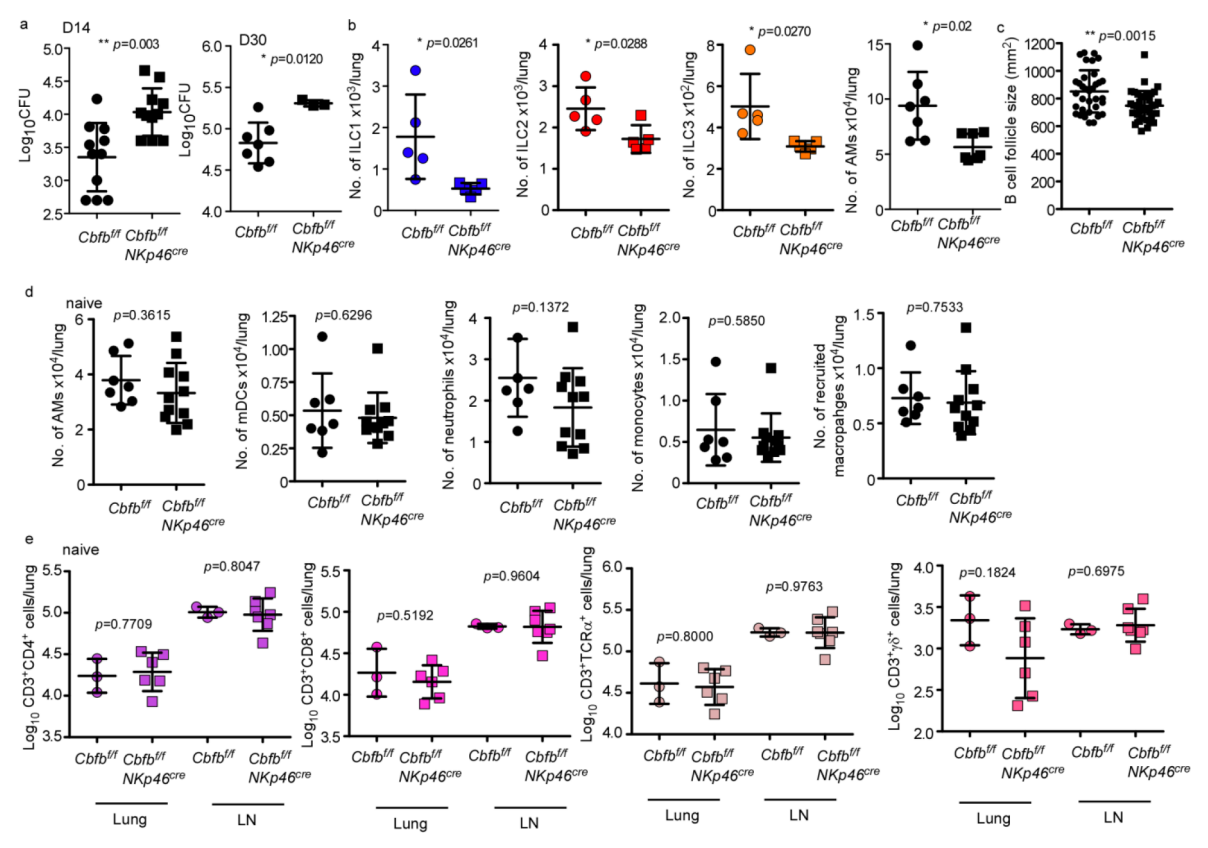
a
D14
** p=0.003
Log10CFU
D30
* p=0.0120
Cbfbf/f
Cbfbf/f NKp46cre
b
* p=0.0261
No. of ILC1 x10^3/lung
* p=0.0288
No. of ILC2 x10^3/lung
* p=0.0270
No. of ILC3 x10^2/lung
* p=0.02
No. of AMs x10^4/lung
c
** p=0.0015
B cell follicle size (mm^2)
d
naive
p=0.3615
No. of AMs x10^4/lung
p=0.6296
No. of mDCs x10^4/lung
p=0.1372
No. of neutrophils x10^4/lung
p=0.5850
No. of monocytes x10^4/lung
p=0.7533
No. of recruited macropahges x10^4/lung
e
naive
p=0.7709
p=0.8047
Log10 CD3+CD4+ cells/lung
p=0.5192
p=0.9604
Log10 CD3+CD8+ cells/lung
p=0.8000
p=0.9763
Log10 CD3+TCRα+ cells/lung
p=0.1824
p=0.6975
Log10 CD3+γδ+ cells/lung
Lung
LN

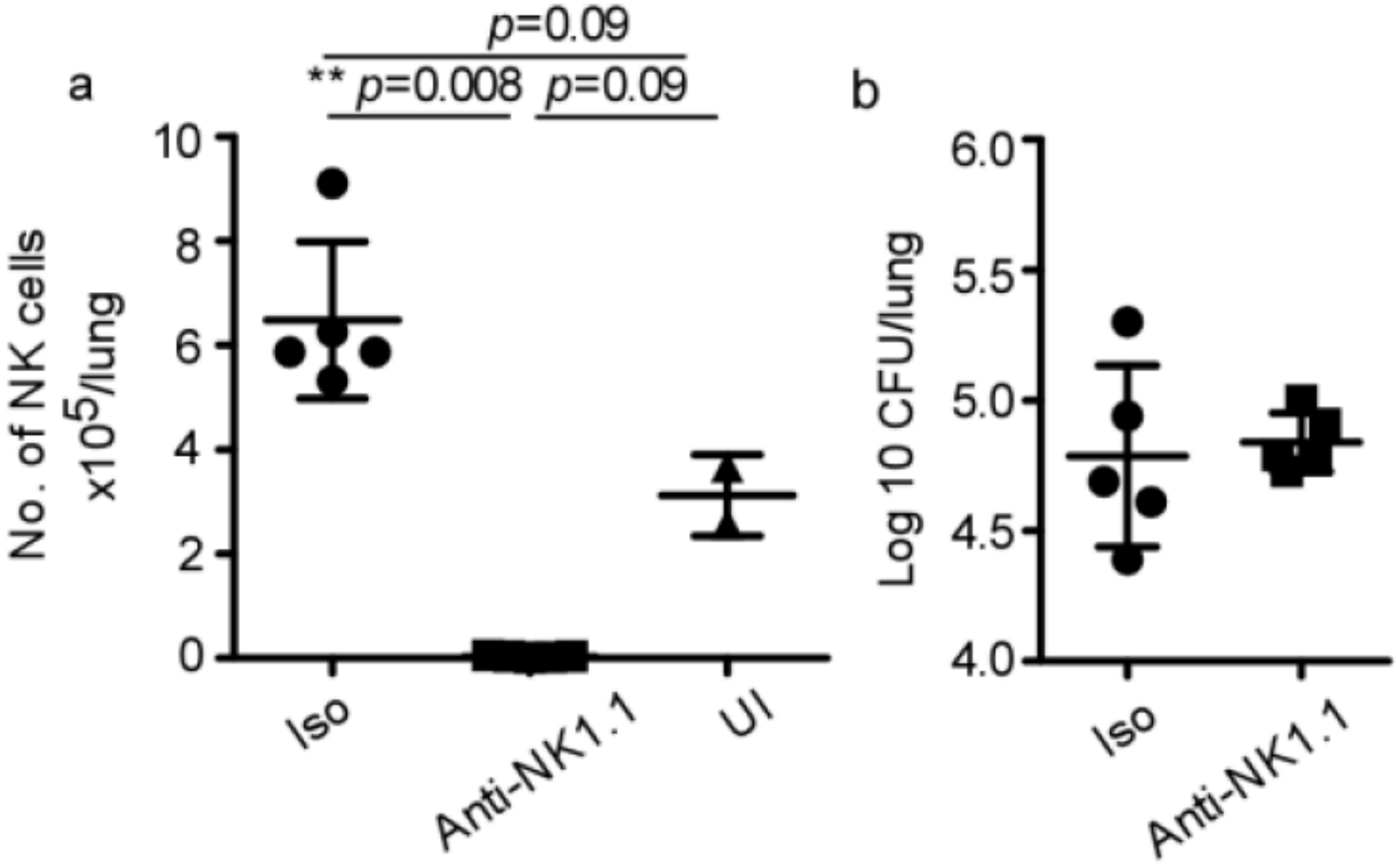
a
p=0.09
** p=0.008
p=0.09
No. of NK cells
x10^5/lung
10
8
6
4
2
0
Iso
Anti-NK1.1
UI
b
Log 10 CFU/lung
6.0
5.5
5.0
4.5
4.0
Iso
Anti-NK1.1

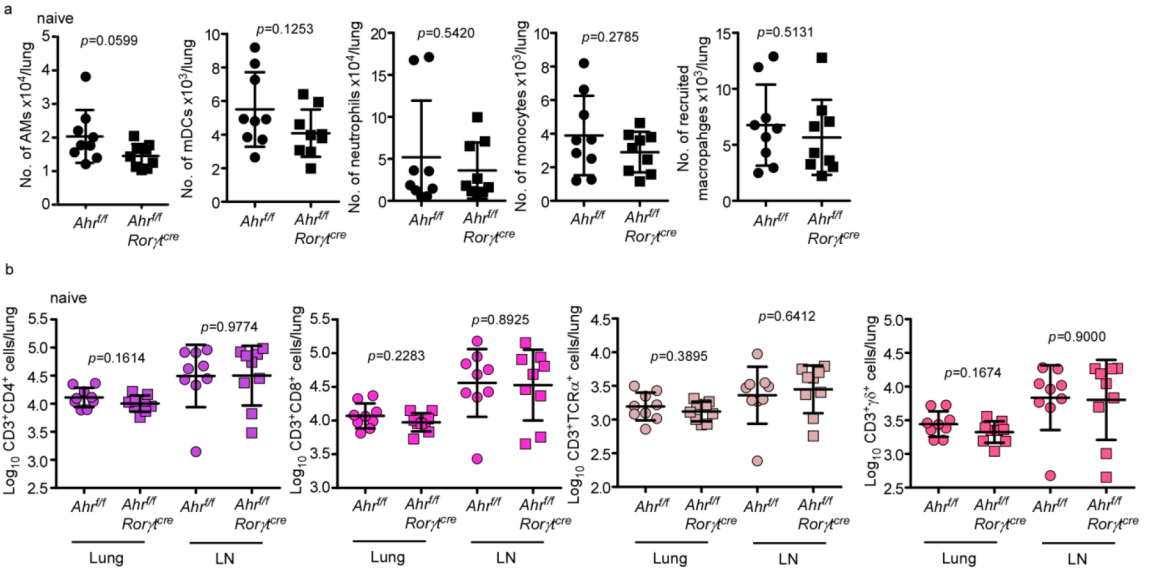
a
naive
No. of AMs x10^4/lung
p=0.0599
No. of mDCs x10^3/lung
p=0.1253
No. of neutrophils x10^4/lung
p=0.5420
No. of monocytes x10^3/lung
p=0.2785
No. of recruited macropahges x10^3/lung
p=0.5131
Ahr f/f
Ahr f/f Rorγt cre
b
naive
Log10 CD3+CD4+ cells/lung
p=0.1614
p=0.9774
Log10 CD3+CD8+ cells/lung
p=0.2283
p=0.8925
Log10 CD3+TCRα+ cells/lung
p=0.3895
p=0.6412
Log10 CD3+γδ+ cells/lung
p=0.1674
p=0.9000
Lung
LN

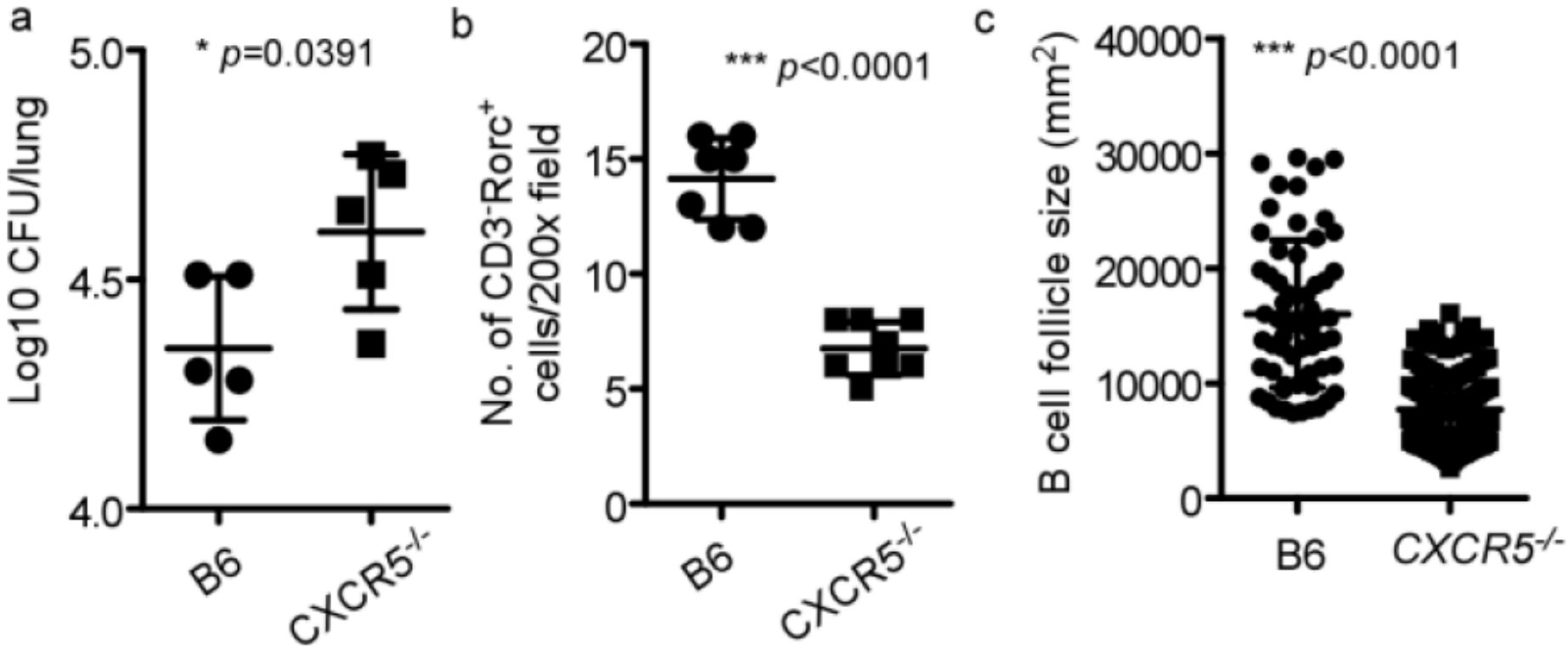
a
5.0
4.5
4.0
Log10 CFU/lung
* p=0.0391
B6
CXCR5-/-
b
20
15
10
5
0
No. of CD3-Rorc+ cells/200x field
*** p<0.0001
B6
CXCR5-/-
c
40000
30000
20000
10000
0
B cell follicle size (mm2)
*** p<0.0001
B6
CXCR5-/-